

Mirror quintic vacua: hierarchies and inflation

Nana Cabo Bizet^{a-b,1}, Oscar Loaiza-Brito^{b,2}, Ivonne Zavala^{c,3}

^a *Mandelstam Institute for Theoretical Physics, School of Physics,
and NITheP, University of the Witwatersrand, WITS 2050, Johannesburg, South Africa*

^b *Departamento de Física, Universidad de Guanajuato,
Loma del Bosque 103, CP 37150, León, Guanajuato, México*

^c *Department of Physics, Swansea University, Singleton Park, Swansea, SA2 8PP, UK*

ABSTRACT

We study the moduli space of type IIB string theory flux compactifications on the mirror of the CY quintic 3-fold in \mathbb{P}^4 . We focus on the dynamics of the four dimensional moduli space, defined by the axio-dilaton τ and the complex structure modulus z . The z -plane has critical points, the conifold, the orbifold and the large complex structure with non trivial monodromies. We find the solutions to the Picard-Fuchs equations obeyed by the periods of the CY in the full z -plane as a series expansion in z around the critical points to arbitrary order. This allows us to discard fake vacua, which appear as a result of keeping only the leading order term in the series expansions. Due to monodromies vacua are located at a given sheet in the z -plane. A dS vacuum appears for a set of fluxes. We revisit vacua with hierarchies among the 4D and 6D physical scales close to the conifold point and compare them with those found at leading order in [1, 2]. We explore slow-roll inflationary directions of the scalar potential by looking at regions where the multi-field slow-roll parameters ϵ and η are smaller than one. The value of ϵ depends strongly on the approximation of the periods and to achieve a stable value, several orders in the expansion are needed. We do not find realisations of single field axion monodromy inflation. Instead, we find that inflationary regions appear along linear combinations of the four real field directions and for certain configurations of fluxes.

May 16, 2016

¹nana@fisica.ugto.mx

²oloaiza@fisica.ugto.mx

³e.i.zavalacarrasco@swansea.ac.uk

Contents

1	Introduction	1
2	Type IIB flux compactification on the mirror quintic	5
2.1	$\mathcal{N} = 1$ SUGRA	5
2.2	The mirror of the quintic in \mathbb{P}^4	8
2.3	Picard-Fuchs equations	11
2.4	Symmetries of the potential	16
3	Mirror quintic flux vacua: hierarchies and inflation	17
3.1	Hierarchies revisited	18
3.2	Search for vacua	22
3.3	Inflationary regions	26
4	Conclusions	32
A	Transition matrices and periods on the symplectic basis	41
B	Hierarchies	43
C	Effect of monodromies on the scalar potential	44

1 Introduction

Type IIB string theory flux compactifications on Calabi-Yau (CY) orientifolds have become a fruitful scenario to construct effective four dimensional models with desirable phenomenological features. These compactifications attracted a lot of attention after the seminal work of Giddings, Kachru and Polchinski (GKP) [1], where a mechanism for stabilisation of the axio-dilaton and the complex structure moduli was found based on the flux superpotential [3, 4]. Moreover, these compactifications provide a rich arena to study phenomenology. Fluxes' backreaction causes the internal CY manifold to be highly warped, as studied in [5] where uncompact flux supergravity solutions near the conifold were found. This opened up the possibility that large hierarchies among the space-time and compactification physical scales can be realised in string theory constructions as discussed in [1]. Using this approach to moduli stabilisation, extensive studies appeared on the

possibility to construct effective 4D models with (meta)stable de Sitter vacua, starting with the work of [6] and/or with regions of moduli space suitable for slow-roll inflation.

Of particular interest are stringy models of inflation with potentially detectable primordial gravitational waves⁴ [8, 9, 10, 11]. These models predict, via the Lyth bound [12], a super-Planckian field excursion and are thus particularly sensitive to ultraviolet corrections through higher dimensional operators and by quantum corrections to the inflaton mass. Therefore a mechanism to prevent such corrections while preserving the inflationary conditions is required. An attractive possibility to address this issue is to invoke a symmetry that forbids large quantum corrections. In particular, the shift symmetry governing axions can provide such a symmetry. The continuous shift symmetry can be broken by non-perturbative effects to a discrete one, as in natural inflation [13], or spontaneously due to couplings to non-trivial background flux for example, giving rise to a realisation of monomial or chaotic inflation [14] with axions [15]. String theoretic embeddings of the later possibility are known as axion monodromy inflation [8, 9].

Of particular interest for our work is F-term axion monodromy, which arises through the F-term in the superpotential [16, 17, 18, 19]. One interesting possibility to realise F-term axion monodromy inflation in string theory⁵ is to use the axion directions of the complex structure moduli [18, 19, 27, 28]. To study the complex structure (CS) moduli space of the internal six dimensional manifold in CY compactifications, one has to study the periods of the CY. These are defined as the integrals of the holomorphic $(3, 0)$ -form over the 3-cycles of the manifold in an integral symplectic basis of $H_3(CY, \mathbb{Z})$. According to the theorem of Landman [29], at certain critical points in the complex structure moduli space, the periods can have a logarithmic or finite order branch cut behaviour. This leads to a monodromy matrix $\mu_i \in Sp(b_3, \mathbb{Z})$ that acts on the periods $\Pi(z)$ when the i -th critical point is encircled. The matrix μ_i has the property $(\mu_i^k - \mathbf{1})^{p+1} = 0$, with $p \leq 3$ where p is the smallest integer so that the r.h.s. is zero. For $p = 0$, $k > 1$ there is an \mathbb{Z}_k orbifold singularity. The cases $k = 1$ are the unipotent cases. The conifold has $p = 1$ and the maximal unipotent case is $p = 3$. In the case of the mirror quintic one has a conifold point, a large complex structure (LCS) point, or maximal unipotent point and a \mathbb{Z}_5^3 orbifold point.

Hence the monodromies around each of the different critical points are of different nature. For example, the monodromy around the orbifold has a finite order. Instead, monodromies around the LCS and conifold points have infinite order. This has triggered interest in these critical points as potential set ups to realise large field inflation in string theory supergravity models, using the mechanism of axion monodromy [8, 9]. Indeed, the Kähler potential is invariant under a shift symmetry, or more generally a monodromy along the argument of the complex structure, $\arg(z) \rightarrow \arg(z) + 2\pi n$, which is broken spontaneously by the fluxes.

⁴Although whether primordial gravitational waves can be realised within perturbative string theory remains an open question [7].

⁵For further recent studies on axion monodromy see [20, 21, 22, 23] and in non-geometric compactifications [24, 25, 26].

A common simplification used in the literature to realise CS axion monodromy in these type of compactifications is to consider only the leading order term in the series expansion of the periods in terms of the CS moduli [18, 23, 30, 31] when computing the scalar potential

$$V = \frac{e^K}{2\kappa_{10}^2 g_s} (|DW|^2 - 3|W|^2),$$

where the periods enter into the superpotential W and the Kähler potential K (see below). However, one may worry that by cutting the series at the leading order might lead to apparent vacua, which disappear when higher order terms are included or miss interesting regions for cosmological applications. In [28] for example, the authors kept up to second order in the periods' expansion and they found interesting new potentials suitable to study natural inflation.

In the present work we consider this problem in detail by studying type IIB orientifold flux compactifications keeping all orders in the series expansion of the periods in the complex structure modulus, necessary to achieve convergence of the solutions we study. To achieve this, we need to keep up to order 600 in the series' expansion. In this sense our computations are exact. We focus on the CY mirror of the quintic on \mathbb{P}^4 [32] and compute the periods of this manifold in four different patches, around the three singular points, and around a regular point, keeping all necessary orders in the series until convergence is achieved. We also obtain the transition functions that allow us to move from one patch to the other, covering the whole CS moduli space.

The CS moduli space of the mirror quintic has been previously studied in [32, 33]. We study the periods around the conifold as in [33], but do this up to a higher order in the series expansion in z , until convergence is achieved in the search for vacua and inflationary regions. We also compute the periods around the orbifold, the LCS and around regular points in the z -plane. The solutions around regular points serve to explore regions close to the boundaries of convergence around the critical points. To date, the periods around the conifold in the integer symplectic basis are only known numerically. This is because the transition matrices (conifold-orbifold, conifold-LCS) can only be determined numerically. Considering all these patches and the transition matrices we study the whole complex structure space in the mirror of the quintic on \mathbb{P}^4 . This method has been used in [34] to study the complex structure space of the 4-fold mirror of the sextic on \mathbb{P}^5 .

Including the higher order terms in the series until convergence is achieved, we accomplish various goals. First, we find global (no-scale) vacua appearing beyond the leading order in z . That is, by obtaining the integer symplectic basis in the whole CS moduli space, we are able to explore the vacua landscape in regions far from the critical points. We verify the existence of hierarchies in the physical scales as found in [1], where they took only the leading order contributions to the periods, $\Pi(z)$. We find a correction of order one to this result. We also find that in general, the exact vacua (i.e. the solutions found keeping all orders in the series until convergence is reached), differ from the near conifold approximation solutions studied in [1] and [2]. We verify that hierarchies are a generic feature of flux compactifications. Finally, we look for inflationary regions, where the

multi-field slow-roll parameters are smaller than unity, by varying the fluxes and moving through the whole moduli space. We find small slow-roll parameters over large moduli regions. These inflationary regions seem to happen generically in a multi-field fashion, such that during inflation there are field's displacements along all of the moduli directions.

As mentioned already, we are interested in the dynamics and properties of the complex structure z , and axio-dilaton τ moduli space. Therefore, we focus on no-scale models of the mirror quintic. This will allow us to explore the CS and the dilaton moduli space in more detail and to identify whether or not the axions associated to these fields can be used as inflaton candidates. In order to stabilize the Kähler moduli, it would be necessary to include non-perturbative contributions to the superpotential⁶ or to add (non)-geometric fluxes. It is interesting to mention that a large number of Kähler moduli could increase the chances to find axionic inflationary regions as recently studied in [36, 37].

The paper is structured as follows. In Section 2 we fix our notation and conventions by reviewing orientifold flux compactifications in type IIB string theory. In 2.1 we write down the relevant $\mathcal{N} = 1$ supergravity action in four dimensions and we describe the integral symplectic basis for the periods. In Section 2.2 we discuss the properties of the mirror quintic CY. Finally in Section 2.3 we describe the procedure to solve the PF equations for the periods in all different patches (orbifold-, LCS-, conifold- and a regular point convergence regions) giving explicitly approximated expressions. We finish Section 2 by describing the monodromies as shift symmetries of the Kähler potential and their breaking by the flux generated superpotential in 2.4. In Section 3 we focus on the scalar potential and describe the vacua that we find for different flux configurations. In Section 3.1 we study the vacua near the conifold in [1, 2] and compare them with the exact vacua that we find⁷. In Section 3.2 we describe in detail the vacua we find inside the conifold convergence region. Finally in 3.3 we explore inflationary regions, where the multi-field slow-roll parameters are small for large regions of the moduli space. We find inflationary regions extending from the conifold- to the orbifold point where no particular direction in the moduli space is favoured. That is, inflation seems to occur generically in a multi-field fashion. In particular, the effective inflationary direction does not seem to occur particularly along any shift symmetric directions ($\arg(z)$ and $\text{Re}(\tau)$). Therefore, we do not see a plausible realisation of axion monodromy inflation in this set up. We show further that the ϵ parameter is very sensitive to the approximation considered for the period's series expansion. We conclude the main text in Section 4 with a discussion of our findings. In Appendix A we discuss the integral symplectic basis for the periods in the different patches and present the relevant transition functions. In Appendix B a correction of one order of magnitude is given to the hierarchy formula of [1]. Finally in Appendix C we give an analytical description of the scalar potential along a SUSY preserving direction for the axio-dilaton ($D_\tau W = 0$), moving with monodromies along the conifold

⁶For example, in [35] parametrically controlled moduli stabilisation of the $h^{1,1} = 51$ Kähler moduli was demonstrated extending the analysis to F-theory [34].

⁷Note again that we refer to the vacua we find taking into account all necessary terms in the series for the periods needed for the solutions to converge.

point.

2 Type IIB flux compactification on the mirror quintic

In this section we review the basic ingredients of four dimensional supergravity which arises from the low energy limit of type IIB string theory compactified on Calabi-Yau (CY) orientifolds with non-trivial RR and NS-NS 3-form fluxes. We describe the integral symplectic basis for the CY periods, which is required for flux quantization. Along the way we fix our notation and conventions.

2.1 $\mathcal{N} = 1$ SUGRA

We start with the ten dimensional effective supergravity action in the Einstein frame⁸ including fluxes and focus on the effective four dimensional action after dimensionally reducing it (see [1] for details). That is, in four dimensions we are interested in the action

$$S_4 = \int d^4x \sqrt{g} \left[\frac{M_{Pl}^2}{2} R - M_{Pl}^2 K_{a\bar{b}} \partial_\mu \Phi^a \partial^\mu \bar{\Phi}^{\bar{b}} + V(\Phi^l) \right], \quad (2.1)$$

where $M_{Pl}^2 = 1/\kappa_4^2 = V_6/(\kappa_{10}^2 g_s^2)$ is the Planck scale, V_6 is the dimensionfull 6D volume, $\kappa_{10}^2 = (2\pi)^7 (\alpha')^4 / 2 \equiv \ell_s^8 / 4\pi$, $\ell_s = \sqrt{2\pi} \alpha'$ the string scale and $g_s = \langle e^\phi \rangle$ the string coupling. The indices a, b run over the moduli fields present, which are the axio-dilaton $\tau = C_0 + i e^\phi$, the complex structure z_i , $i = 1, \dots, h^{2,1}$ and the Kähler moduli, T_m , $m = 1, \dots, h^{1,1}$. The Kähler potential for the moduli is given by

$$K = -\ln[-i(\tau - \bar{\tau})] - \ln \left[i \int_{CY} \Omega \wedge \bar{\Omega} \right] - 2 \ln[\mathcal{V}], \quad (2.2)$$

where Ω is the holomorphic $(3,0)$ form of the CY and \mathcal{V} is the dimensionless volume defined in terms of the dimensionless Kähler moduli T_m .

The complex structure moduli can be parameterised by the integrals of Ω over a canonical homology basis of the CY. These are known as the periods, Π of the CY. In this work according to [38] we use the canonical integral symplectic basis (α_I, β^I) on $H^3(CY, \mathbb{Z})$ and its dual homology basis (A^I, B_I) of $H_3(CY, \mathbb{Z})$ satisfying

$$\int_{CY} \alpha_I \wedge \beta^J = \delta_I^J = - \int_{CY} \beta^J \wedge \alpha_I, \quad \int_{CY} \alpha_I \wedge \alpha_J = \int_{CY} \beta^I \wedge \beta^J = 0, \quad (2.3)$$

$$\int_{A^J} \alpha_I = - \int_{B_I} \beta^J = \delta_I^J. \quad (2.4)$$

⁸We use the conventions for transforming to the Einstein frame $G_{MN}^E = e^{(\phi - \phi_0)/2} G_{MN}^s$, where G_{MN} is the 10D metric, $\langle e^\phi \rangle = e^{\phi_0} = g_s$ with ϕ the dilaton and g_s is the string coupling. With these conventions the volumes are conformally invariant.

The indices I and J run from 0 to $h^{2,1}$. With respect to this basis the CY periods are defined as

$$\Pi = \begin{pmatrix} \mathcal{X}^I \\ \mathcal{F}_I \end{pmatrix} = \begin{pmatrix} \int_{A^I} \Omega \\ \int_{B_I} \Omega \end{pmatrix}, \quad (2.5)$$

and consequently, the holomorphic 3-form can be expanded as

$$\Omega = \mathcal{X}^I \alpha_I - \mathcal{F}_I \beta^I. \quad (2.6)$$

Similarly the Kähler potential for the complex structure moduli is given by

$$K_{CS} = -\ln(-i \bar{\Pi}^T \Sigma \Pi), \quad (2.7)$$

where Σ denotes the symplectic matrix, defined as

$$\Sigma = \begin{pmatrix} 0 & \mathbb{1}_{k \times k} \\ -\mathbb{1}_{k \times k} & 0 \end{pmatrix},$$

with $k = 1 + h^{2,1}$.

In the following we shortly review the integral symplectic basis (2.5) which is required for flux quantization. This basis is the one employed through the paper in all the different patches in the CS moduli space. Special geometry implies the existence of a holomorphic prepotential \mathcal{F} , which is homogeneous of degree two in the \mathcal{X}^I . The \mathcal{F}_I are given as derivatives $\mathcal{F}_I = \frac{\partial \mathcal{F}}{\partial \mathcal{X}^I}$. The prepotential determines the periods, the couplings, as well as the Kähler potential, see e.g. [39]. Mirror symmetry implies that at the large radius point of a CY 3-fold M_3 , corresponding to the large complex structure (LCS) point on the mirror W_3 the prepotential reads as follows [39, 40]

$$\begin{aligned} \mathcal{F} &= -\frac{C_{ijk}^0 \mathcal{X}^i \mathcal{X}^j \mathcal{X}^k}{3! \mathcal{X}^0} + n_{ij} \frac{\mathcal{X}^i \mathcal{X}^j}{2} + c_i \mathcal{X}^i \mathcal{X}^0 - i \frac{\chi \zeta(3)}{2(2\pi)^3} (\mathcal{X}^0)^2 + (\mathcal{X}^0)^2 f(q) \\ &= (\mathcal{X}^0)^2 \tilde{\mathcal{F}} = (\mathcal{X}^0)^2 \left[-\frac{C_{ijk}^0 t^i t^j t^k}{3!} + n_{ij} \frac{t^i t^j}{2} + c_i t^i - i \frac{\chi \zeta(3)}{2(2\pi)^3} + f(q) \right], \end{aligned} \quad (2.8)$$

where $i, j, k = 1, \dots, h^{2,1}$, $q_i = \exp(2\pi i t_i)$, $f(q)$ represents the instanton contributions, C_{ijk}^0, c_{ij}, n_i and χ are topological data of the manifold [34]. The integral basis for the periods at the LCS point is then given by

$$\Pi_{LCS} = \begin{pmatrix} \mathcal{X}^0 \\ \mathcal{X}^i \\ \mathcal{F}_0 \\ \mathcal{F}_i \end{pmatrix} = \mathcal{X}^0 \begin{pmatrix} 1 \\ t^i \\ 2\tilde{\mathcal{F}} - t^i \partial_i \tilde{\mathcal{F}} \\ \frac{\partial \tilde{\mathcal{F}}}{\partial t^i} \end{pmatrix} = \mathcal{X}^0 \begin{pmatrix} 1 \\ t^i \\ \frac{C_{ijk}^0 t^i t^j t^k}{3!} + c_i t^i - i \frac{\chi \zeta(3)}{(2\pi)^3} + f(q) \\ -\frac{C_{ijk}^0}{2} t^i t^j + n_{ij} t^j + c_i + \partial_i f(q) \end{pmatrix}. \quad (2.9)$$

The mirror map reads $t^i = \frac{\mathcal{X}^i}{\mathcal{X}^0} = \frac{1}{2\pi i} (\log(z_i) + \Sigma^i(z))$, $i = 1, \dots, h^{2,1}$, where z_i are the complex structure moduli and $\Sigma^i(z)$ are power series in z_i . In Section 2.2 we describe such LCS point for the CY 3-fold mirror of the quintic on \mathbb{P}^4 which is the compactification employed. For this case

$h^{2,1} = 1$, $C_{111}^0 = 5$, $c_1 = \frac{50}{24}$, $n_{11} = -\frac{11}{2}$ and $\chi(W_3) = 200$. We are interested however on other critical points, in particular the conifold, close to which the periods have to be determined, and one needs to obtain their expressions in terms of the integer symplectic basis (2.9).

Turning on fluxes in the different 3-cycles of an orientifold CY, generates a four dimensional scalar potential for the axio-dilaton and the complex structure moduli, given by [1],

$$V = \frac{1}{2\kappa_{10}^2} \int_{CY} d^6y \sqrt{\tilde{g}} \frac{G_{(3)} \cdot \bar{G}_{(3)}}{12 \text{Im } \tau} - \frac{i}{4\kappa_{10}^2 \text{Im } \tau} \int_{CY} G_3 \wedge \bar{G}_3, \quad (2.10)$$

where the inner product of the three-form fluxes is performed using \tilde{g}_{mn} given by Eq. (3.7) below. The first contribution comes from the fluxes and the second from the branes and orientifold charges. The 3-form flux $G_{(3)}$ is defined in terms of the RR, NS-NS flux and dilaton as:

$$G_{(3)} = F_{(3)} - \tau H_{(3)}, \quad (2.11)$$

with

$$F_{(3)} = F_{(3)}^I \alpha_I - F_{(3)I} \beta^I, \quad H_{(3)} = H_{(3)}^I \alpha_I - H_{(3)I} \beta^I, \quad (2.12)$$

so that

$$G_{(3)} = F_{(3)} - \tau H_{(3)} = G^I \alpha_I - G_I \beta^I, \quad (2.13)$$

with $G^I = F_{(3)}^I - \tau H_{(3)}^I$ and $G_I = F_{(3)I} - \tau H_{(3)I}$.

The $F_{(3)}, H_{(3)}$ fluxes on the 3-cycles of the orientifold CY are quantised as

$$\begin{aligned} \frac{1}{(2\pi)^2 \alpha'} \int_{A^I} F_{(3)} &= M^I, & \frac{1}{(2\pi)^2 \alpha'} \int_{A^I} H_{(3)} &= N^I, \\ \frac{1}{(2\pi)^2 \alpha'} \int_{B_I} F_{(3)} &= M_I, & \frac{1}{(2\pi)^2 \alpha'} \int_{B_I} H_{(3)} &= N_I. \end{aligned} \quad (2.14)$$

Note that due to the Dirac quantization condition the fluxes need to be defined with respect to an integral basis of $H^3(CY, \mathbb{Z})$ given in (2.9). The scalar potential (2.10) can be written in an $\mathcal{N} = 1$ supergravity form as

$$V = \frac{1}{2\kappa_{10}^2 g_s} e^K \left[K^{a\bar{b}} D_a W \bar{D}_{\bar{b}} \bar{W} - |W|^2 \right], \quad (2.15)$$

The scalar potential (2.15) depends on the superpotential W and the Kähler potential. In (2.15) the indices a, b denotes the moduli fields, $K^{a\bar{b}}$ is the inverse metric in field space and $D_a W = \partial_a W + \partial_a K W$ is the supersymmetric covariant derivative of W . The superpotential generated by the fluxes is given by the Gukov-Vafa-Witten (GVW) superpotential [3]:

$$\begin{aligned} W &= \int_{CY} G_{(3)} \wedge \Omega = \int_{CY} (F_{(3)} - \tau H_{(3)}) \wedge \Omega, \\ &= (F_{(3)}^I - \tau H_{(3)}^I) \mathcal{F}_I - (F_{(3)I} - \tau H_{(3)I}) \mathcal{X}^I = G \Sigma \Pi, \end{aligned} \quad (2.16)$$

where in an abuse of notation, we have omitted the use of explicit indices in the last expression and we have defined $\int_{A^I, B_J} G_{(3)} = G = (G^I, G_J)$ where the fluxes are defined through (2.14) (that is e.g. $\int_{A^I} F_{(3)} = M^I (2\pi)^2 \alpha' \equiv F_{(3)}^I$).

We consider non-supersymmetric no-scale models [1] where the the Kähler moduli cancel the negative contribution to (2.15) by setting $K^{m\bar{n}} D_m W \bar{D}_{\bar{n}} \bar{W} - 3|W|^2 = 0$. Since in this case the GVW superpotential depends only on the dilaton and the complex structure moduli the scalar potential is positive definite with the form

$$V = \frac{1}{2\kappa_{10}^2 g_s} e^K \left[K^{i\bar{j}} D_i W \bar{D}_{\bar{j}} \bar{W} \right]. \quad (2.17)$$

The indices run only over the axio-dilaton and the complex structure modulus. This is the potential that we study in the rest of the paper. As already mentioned, for our analysis we shall not consider the stabilisation of the Kähler moduli. In the case of the mirror quintic $h^{2,1} = 1$ and we use the following notation for the components of the periods and the fluxes:

$$\Pi = \begin{pmatrix} \mathcal{X}^I \\ \mathcal{F}_I \end{pmatrix} = \begin{pmatrix} \Pi_1 \\ \Pi_2 \\ \Pi_3 \\ \Pi_4 \end{pmatrix}, \quad (2.18)$$

$$\begin{aligned} (F_{(3)}^I, F_{(3)I}) &= (F_1, F_2, F_3, F_4), \\ (H_{(3)}^I, H_{(3)I}) &= (H_1, H_2, H_3, H_4), \\ (G_{(3)}^I, G_{(3)I}) &= (G_1, G_2, G_3, G_4). \end{aligned} \quad (2.19)$$

2.2 The mirror of the quintic in \mathbb{P}^4

We consider the explicit orientifold compactification of type IIB string theory where the internal manifold is the mirror of the quintic hyper surface on \mathbb{P}^4 [32]. We start by describing the properties of the CY manifold. In particular, we describe the critical points in the complex structure moduli space of the manifold, namely the orbifold, large complex structure and conifold singularities and the structure of the monodromies as one encircles these critical points. We shall describe how to compute the periods for this manifold in the vicinity of those singular points, covering thus the full complex structure moduli space. We use these results in the next section to explore new vacua and their properties, as well as potential regions to realise slow-roll inflation. Let us first review the construction of the mirror of the quintic CY in \mathbb{P}^4 following [32]. The quintic CY is the 3-fold constructed as the most general quintic hyper surface $\tilde{P} = 0$ in \mathbb{P}^4 . This variety has 101 complex structure moduli corresponding to the independent coefficients entering \tilde{P} . It further has a single Kähler modulus and hence Euler number given by $\chi = (2h^{1,1} - h^{2,1}) = -200$.

The mirror of the quintic CY threefold is obtained by modding out a \mathbb{Z}_5^3 symmetry from a one parameter family of polynomials on \mathbb{P}^4 . This family is given by

$$W_\psi = \left\{ (x_1, x_2, x_3, x_4, x_5) \in \mathbb{P}^4, P = \sum_{k=1}^5 x_k^5 - 5\psi \prod x_k = 0 \right\}. \quad (2.20)$$

W_ψ has a \mathbb{Z}_5^3 symmetry generated by phase rotations $x_l \rightarrow e^{\frac{2\pi i g^{(k)}}{5}} x_l$, $l = 1, \dots, 5$ with $g^{(1)} = (0, 1, 0, 0, 4)$, $g^{(2)} = (0, 0, 1, 0, 4)$ and $g^{(3)} = (0, 0, 0, 1, 4)$. The symmetry [32] is modded out to obtain the mirror quintic manifold: W_ψ/\mathbb{Z}_5^3 . In the mirror manifold, the parameter of the invariant deformation ψ constitutes the single complex structure modulus. As dictated by mirror symmetry, the mirror quintic has $h^{1,1} = 101$ Kähler moduli, a single complex structure modulus, $h^{2,1} = 1$, which we denote by $z = \psi^5$ and Euler number $\chi = +200$. It also has Betti number $b_3 = \sum_{i=0}^3 h^{3-i,i} = 4$, that is, four 3-cycles where the three-form fluxes can be turned on. Therefore it has four periods (2.5), which are all functions of the single complex structure modulus z . There are three critical points in the complex structure moduli space, the orbifold, the conifold and the large complex structure. Both the conifold and the large complex structure points arise when

$$P = dP = 0. \quad (2.21)$$

The conifold arises at the locus $\forall_i 5x_i^5 - 5\psi x_1 x_2 x_3 x_4 x_5 = 0$, which is satisfied for $\psi^5 = 1$ and $|x_i| = 1$. At this point the CY has a nodal singularity. The modulus ψ can be parametrized by the coordinate z_C given as $z_C = 1 - \psi^{-5}$. At the point $\psi \rightarrow \infty$, the manifold degenerates to $x_1 x_2 x_3 x_4 x_5 = 0$. This is the large complex structure point (LCS) also called the maximal unipotent monodromy (MUM) point located at $z_C = 1$. Finally the point $\psi = 0$ corresponds to an specially symmetric point, the orbifold, located at $z_C = \infty$. Transport of the periods around the critical points $\psi_0 = 0, 1, \infty$, lead to specific monodromy transformations:

$$\Pi \rightarrow \mu \Pi, \quad (2.22)$$

where μ is the monodromy transformation matrix. We denote the monodromies around the conifold, the large complex structure and the orbifold points by μ_C, μ_M and μ_O respectively. The monodromy around the LCS ($\psi_0 = \infty$) fulfills the condition $(\mu_M - 1)^4 = 0$, which means that this is a point of maximal unipotent monodromy. The monodromy μ_M is of infinite order, which implies that at every turn around $\psi_0 = \infty$ the periods acquire different values. Around the orbifold point ($\psi_0 = 0$) the monodromy satisfies $\mu_O^5 = 1$, and it is therefore of order 5. Finally, around the conifold point $\psi_0 = 1$, we have $(\mu_C - 1)^2 = 0$ and this point is unipotent. Also μ_C is of infinite order. The periods (2.5) obey Picard-Fuchs (PF) equations, whose solutions give the dependence on the complex structure modulus that will be explored in Section 2.3. From the explicit expressions of the periods the matrices μ_O, μ_C, μ_M can be obtained in any given basis, we will write them in terms of the integral symplectic basis in (2.39) and (2.40).

The mirror quintic W_ψ/\mathbb{Z}_5^3 possesses a symmetry which identifies $x_1 \leftrightarrow x_2$ leading to the possibility of having $O7$ planes and $O3$ -planes [41]. A fixed hyperplane under this symmetry is given by

$$(x_1, x_1, x_3, x_4, x_5) \in \mathbb{P}^4 \text{ with } 2x_1^5 + x_3^5 + x_4^5 + x_5^5 - 5\psi x_1^2 x_3 x_4 x_5 = 0, \quad (2.23)$$

which has two complex internal dimensions and represents an $O7$ plane. Additionally the locus $(1, -1, 0, 0, 0)$, which is also fixed under $x_1 \leftrightarrow x_2$ constitutes an $O3$ plane. That is, the $O7$ plane divisor is given by $x_1 - x_2 = 0$, and an $O3$ plane appears at the point $x_1 = -x_2 = 1, x_3 = x_4 = x_5 = 0$.

Therefore the mirror quintic orientifold compactification contains $O3$ and $O7$ -planes. In order to cancel tadpoles in this set-up we should also include spacetime filling $D7$ -branes, as well as $D3$ -branes. We make here a short review of [42] applied to our setup. The 3-form fluxes contribute to the $D3$ -brane charge tadpole and therefore we have

$$\begin{aligned} N_{flux} &= \frac{1}{2\kappa_{10}^2 T_3} \int_{CY} F_3 \wedge H_3 = -\frac{g_s}{(2\pi)^4 (\alpha')^2} F \cdot \Sigma \cdot H, \\ &= \frac{N_{O3}}{2} - 2N_{D3} + \frac{\chi(D_{O7})}{6} + \sum_a (Q_{D7}^a + Q_{D7}^{'a}), \\ &= \frac{N_{O3}}{2} - 2N_{D3} + \frac{\chi(D_{O7})}{6} + \sum_a N_a \frac{\chi(D_a)}{12}, \end{aligned} \quad (2.24)$$

where $T_3 = (g_s(\alpha')^2(2\pi)^3)^{-1}$ is the $D3$ -brane tension, the index a numerates the $D7$ branes, D_a is the divisor wrapped by the $D7$ brane, $\chi(D_a)$ the corresponding Euler number, D_{O7} is the divisor that corresponds to the $O7$ plane, $2N_{D3}$ is the number of $D3$ branes and their images. $\chi(D_{O7})$ is computed via [42]

$$\chi(D_{O7}) = \int_{CY} c_2(D_{O7}) \wedge [D_{O7}], \quad (2.25)$$

with c_2 the second Chern class of the divisor D_{O7} . The calculation of $\chi(D_{O7})$ is involved because of the presence of 101 Kähler moduli. The $D7$ tadpole cancellation reads [42]

$$\sum_a N_a ([D_a] + [D_a']) = 8[D_{O7}], \quad (2.26)$$

where D_a' is its image under the orientifold projection of D_a .

When the $D7$ branes are on top of the $O7$ plane we have $[D_a] = [D_a'] = [D_{O7}]$, this simplifies the equation (2.26) to $\sum_a N_a = 4$. In this case there is a zero contribution from the branes to the superpotential and the Kähler potential $W_{D7} = 0$ (see (4.57) in [43]) and $K_{D7} = 0$ (see (4.26) in [43]) avoiding a mixture with CS moduli. The $D3$ brane tadpole cancellation condition (2.24) reduces to

$$N_{flux} = \frac{N_{O3}}{2} + \frac{\chi(D_{O7})}{2} - 2N_{D3}. \quad (2.27)$$

In what follows we assume for our study that by incorporating the necessary number of $D3$ -branes and by computing the Euler number of the divisors in the mirror quintic, it is possible to cancel the tadpole (2.24) or (2.27) for any flux configuration.

2.3 Picard-Fuchs equations

In this section we write the Picard-Fuchs (PF) equations, which are fourth order differential equations, satisfied by the periods, in four different coordinates systems. Three of those correspond to convenient coordinates near the critical points of the complex structure moduli space: the orbifold, conifold and large complex structure points. The other coordinates system is defined near a regular point in the CS moduli space. This system is convenient to study the periods close to the boundaries of convergence from the critical points patches. We describe the power series and logarithmic solutions in each of the patches and the method to obtain the transition matrices to the integral symplectic basis (2.9). This moduli space has been studied previously in [33, 38]. In [33] the periods near the conifold were obtained. Here we are interested in having the period series up to an arbitrary order in all different patches, and for this we also compute the transition matrices between all of those patches.

Let us start by looking at the PF equations on the vicinity of the LCS point. A change of coordinates from ψ to ψ^{-5} in W_ψ/\mathbb{Z}_5^3 was used in [38]. Here we instead use the variable $z_M = \psi^{-5}5^{-5}$. We label the variable with a subindex M because the LCS ($\psi = \infty$ i.e. $z_M = 0$) is a point of MUM. Using this variable, the PF equation takes the form

$$(\theta_M^4 - z_M(\theta_M + a_1)(\theta_M + a_2)(\theta_M + a_3)(\theta_M + a_4))\pi_{M,i} = 0, \quad i = 1, 2, 3, 4, \quad (2.28)$$

with $\pi_{M,i}$ the solutions on the LCS basis, $\theta_M = z_M \partial_{z_M}$ and $a_k = k/5$, $k = 1, 2, 3, 4$.

The next change of variables we do is $z_O = 1/z_M$. We denote this as the orbifold basis since the orbifold point is located at $z_O = 0$. The PF equations in these coordinates read

$$(-z_O/5^5 \theta_O^4 + (a_1 - \theta_O)(a_2 - \theta_O)(a_3 - \theta_O)(a_4 - \theta_O))\pi_{O,i} = 0, \quad i = 1, 2, 3, 4, \quad (2.29)$$

with $\theta_O = z_O \partial_{z_O}$ and $\pi_{O,i}$ the solutions in the orbifold basis.

The most relevant coordinate system for our discussion, is defined as $z_C = (1 - z_M 5^5)$ denoting the conifold basis with the conifold singularity located at $z_C = 0$. Making the change of variables in (2.28) we obtain the PF equations

$$(\theta_C^4 - (1 - z_C)(a_1 - \theta_C)(a_2 - \theta_C)(a_3 - \theta_C)(a_4 - \theta_C))\pi_{C,i} = 0, \quad i = 1, 2, 3, 4, \quad (2.30)$$

where $\pi_{C,i}$ are the solutions in the conifold basis and $\theta_C = (z_C - 1)\partial_{z_C}$. The three different coordinates are related to each other via $z_M = 1/z_O = 5^{-5}(1 - z_C)$. In the coordinates described above around the conifold, LCS and orbifold points, the convergence radii of the period series

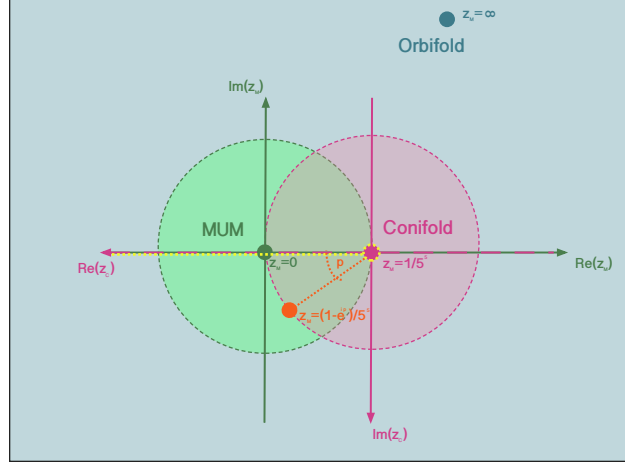


Figure 1: The figure represents the three different critical points of the CS moduli space of the mirror of the quintic CY on \mathbb{P}^4 on the complex z_M plane. As well we represent the regular point where we also constructed the solution to the PF equation in order to improve convergence, $z_M = (1 - e^{ip})/5^5$ with $-\pi/3 < p < \pi/3$. The yellow dashed line represents the branch cut chosen for the conifold periods. Recall that $z_C = 1 - 5^5 z_M$ and $z_O = 1/z_M$. The LCS, conifold and orbifold series convergence regions are coloured in green, pink and blue respectively.

solution are 1, 5^{-5} and 5^5 respectively. Let us also write the PF equations in the vicinity of an arbitrary point lying on the boundary of the conifold convergence region. That is, we write the conifold coordinates of that point as $z_C^0 = e^{i\alpha}$. These new coordinates allow us to study the potential with precision close to the limit of convergence of the conifold coordinates. We represent the critical points as well as this regular point in Figure 1.

The coordinates of a given point in the conifold and α coordinates are related as $z_C = z_\alpha + e^{i\alpha}$. Making this change of variable in (2.30) one obtains the PF equations in terms of the z_α coordinates:

$$(\theta_\alpha^4 - (1 - z_\alpha - e^{i\alpha})(a_1 - \theta_\alpha)(a_2 - \theta_\alpha)(a_3 - \theta_\alpha)(a_4 - \theta_\alpha))\pi_i^\alpha = 0, \quad i = 1, 2, 3, 4, \quad (2.31)$$

where π_i^α are the solutions in the regular point basis and $\theta_\alpha = (z_\alpha + e^{i\alpha} - 1)\partial_{z_\alpha}$. The point $\alpha = \pi$ constitutes the LCS point. The convergence radius of the series power solutions around $e^{i\alpha}$ is 1. We solve the PF equations in the vicinity of the points $e^{i\alpha}$. For this set of points, there is convergence of both the LCS and conifold coordinate series when $-\pi/3 < \alpha < \pi/3$. This reads

$$z_\alpha = e^{i\alpha} - e^{i\pi/3}, \quad z_M = 1 - e^{i\alpha}, \quad z_C = e^{i\alpha}, \quad -\pi/3 < \alpha < \pi/3.$$

This extra coordinate system serves in the study of vacua which are very close to the conifold or LCS convergence regions. We use them to discard fake solutions appearing as a consequence of cutting the series of the periods without achieving convergence.

Solving the PF equations

The solutions to the PF equations are generalised hypergeometric functions [38, 44] and have been previously studied in the literature in different bases. In [38] the authors studied the periods in the LCS and orbifold convergence regions and gave an analytic expression valid for both regions. In [33] the authors computed the periods on the conifold convergence region and the transformation matrix to the integral symplectic basis, they explicitly gave the series to order five. Here we determine the solutions near all the critical points and in particular near the conifold point, up to order 600. This allows us to achieve convergence in our calculations when looking for vacua and inflationary regions. The transition matrices that we compute in this way, match those in [33]. In the following we describe how to obtain the solutions of the PF equations in the bases z_M, z_C, z_O described previously, and the Ansätze employed.

Through this section we denote the independent solutions of the PF equations by π , while recall that Π denotes the periods in the integral symplectic basis (2.9). First, we search for solutions near the conifold point, making the power series Ansatz

$$\pi_{C,i} = z_C^x (c_0 + c_1 z_C + c_2 z_C^2 + \cdots + c_n z_C^n), \quad i = 1, 2, 3. \quad (2.32)$$

Applying the PF operator (2.30) to (2.32), the solutions for the initial equation are $x = 0, 1^2, 2$. The degeneracy of x at $x = 1$ indicates the existence of a logarithmic solution. This solution vanishes when $z_C \rightarrow 0$ and can be constructed as

$$\pi_{C,4} = z_C (c_0 + c_1 z_C + c_2 z_C^2 + \cdots + c_n z_C^n) \ln z_C + z_C^x (b_0 + b_1 z_C + b_2 z_C^2 + \cdots). \quad (2.33)$$

Substituting (2.32) into (2.28) we obtain a set of recursive equations for the coefficients to each order in the expansion. For example, in the case $x = 0$ the first two equations are

$$\begin{aligned} 0 &= \frac{19 c_0}{5} - \frac{74 c_1}{5} + 12 c_2, \\ 0 &= -\frac{5399 c_0}{625} + 66 c_1 - \frac{642 c_2}{5} + 72 c_3. \end{aligned} \quad (2.34)$$

The system of equations is solved recursively. To order six, we obtain the expressions

$$\begin{aligned} \pi_{C,1} &= 1 + \frac{2}{5^4} z_C^3 + \frac{97}{2 \cdot 3 \cdot 5^4} z_C^4 + \frac{2971}{2 \cdot 3 \cdot 5^5} z_C^5 + \frac{13 \cdot 1175173}{2 \cdot 3 \cdot 5^{11} \cdot 7} z_C^6 + O(z_C^7), \\ \pi_{C,2} &= z_C + \frac{7}{10} z_C^2 + \frac{41}{75} z_C^3 + \frac{1133}{4 \cdot 5^4} z_C^4 + \frac{6089}{5^6} z_C^5 + \frac{7 \cdot 13 \cdot 29 \cdot 61}{2 \cdot 3 \cdot 5^7} z_C^6 + O(z_C^7), \\ \pi_{C,3} &= z_C^2 + \frac{37}{30} z_C^3 + \frac{2309}{1800} z_C^4 + \frac{31 \cdot 9241}{2^3 \cdot 3^2 \cdot 5^5} z_C^5 + \frac{41932661}{2^4 \cdot 3^3 \cdot 5^7} z_C^6 + O(z_C^7), \\ \pi_{C,4} &= -\frac{23}{360} z_C^3 - \frac{6397}{3 \cdot 10^6} z_C^4 - \frac{333323}{2^5 \cdot 5^7} z_C^5 + \frac{103 \cdot 353 \cdot 929}{2^5 \cdot 5^7} z_C^6 + \pi_{C,2} \ln z_C + O(z_C^7). \end{aligned} \quad (2.35)$$

To achieve convergence in our calculations, we use the solutions (2.35) up to order 600 in our analysis. The convergence radius of the power series is obtained from the formula $\lim_{n \rightarrow \infty} |c_n/c_{n+1}| = 1$ and similarly for b_n , $\lim_{n \rightarrow \infty} |b_n/b_{n+1}| = 1$. The expressions (2.35) for the periods near the conifold are particularly useful for our study⁹.

Let us now study the solutions of the PF equations near the orbifold (2.29). This set of solutions is also obtained by starting with an ansatz $\pi_{O,i} = z_O^x (c_0 + c_1 z_O + c_2 z_O^2 + \dots)$ and applying to it the PF operator (2.29). The terms multiplying each power of z need to vanish. From the z^0 term one gets $\prod_{i=1}^4 (x - i/5) = 0$, giving the x solutions $x = \frac{1}{5}, \frac{2}{5}, \frac{3}{5}$ and $\frac{4}{5}$. For every value of x we plug the ansatz back into (2.29) and make some coefficients choice, to obtain the solutions

$$\begin{aligned}\pi_{O,1} &= z_O^{1/5} + \frac{1}{2^3 \cdot 3 \cdot 5^6} z_O^{6/5} + \frac{3}{2^3 \cdot 5^{12} \cdot 7} z_O^{11/5} + O(z_O^{16/5}), \\ \pi_{O,2} &= z_O^{2/5} + \frac{2}{3^2 \cdot 5^6} z_O^{7/5} + \frac{2401}{2^3 \cdot 3^4 \cdot 5^{12} \cdot 11} z_O^{12/5} + O(z_O^{17/5}), \\ \pi_{O,3} &= z_O^{3/5} + \frac{27}{2^3 \cdot 5^6 \cdot 7} z_O^{8/5} + \frac{64}{5^{12} \cdot 7 \cdot 11} z_O^{13/5} + O(z_O^{18/5}), \\ \pi_{O,4} &= z_O^{4/5} + \frac{16}{2^2 \cdot 13 \cdot 631} z_O^{9/5} + \frac{1458}{5^{12} \cdot 7 \cdot 11 \cdot 13} z_O^{14/5} + O(z_O^{19/5}).\end{aligned}\tag{2.36}$$

We proceed in a similar fashion to find the solutions near the LCS point in the z_M variables. That is, we start by making a power series Ansatz $\pi_{M,1} = z^x (c_0 + c_1 z + c_2 z^2 + \dots)$ plug it into (2.28) and find the solutions $\pi_{M,1}$. As before, the degeneracy of x in the solutions to the initial equation $x^4 = 0$, coming from the z^0 power, indicates the presence of logarithmic solutions. One continues then with three additional Ansätze $\pi_{M,2}, \pi_{M,3}$ and $\pi_{M,4}$, such that all π_M have a polynomial term w_M^0, w_M^1, w_M^2 and w_M^3 . The solutions to equation (2.28) in the LCS point vicinity are then given by

$$\begin{aligned}\pi_{M,1} &= w_M^0, \\ \pi_{M,2} &= w_M^1 + w_M^0 \ln z_M, \\ \pi_{M,3} &= \frac{5}{2} w_M^2 + \frac{5}{2} w_M^0 (\ln z_M)^2 + 5 w_M^1 \ln z_M, \\ \pi_{M,4} &= \frac{5}{6} w_M^3 + \frac{5}{6} w_M^0 (\ln z_M)^3 + \frac{5}{2} w_M^1 (\ln z_M)^2 + \frac{5}{2} w_M^2 \ln z_M,\end{aligned}\tag{2.37}$$

where the power series in them are obtained to be

$$\begin{aligned}w_M^0 &= \pi_{M,1} = 1 + 120 z_M + 113400 z_M^2 + O(z_M^3), \\ w_M^1 &= 770 z_M + 810225 z_M^2 + O(z_M^3), \\ w_M^2 &= 2875 z_M + \frac{21040875 z_M^2}{4} + O(z_M^3), \\ w_M^3 &= -5750 z_M - \frac{16491875 z_M^2}{4} + O(z_M^3).\end{aligned}$$

⁹In [38] an analytic integral expression for the periods valid in the orbifold and LCS convergence region was given. For our exploration this expression is not enough, because we are interested in looking at the behaviour of the potential near the conifold.

From (2.37) one can write the explicit form of the monodromy in this basis¹⁰. In this way it is possible to compute the periods fully in the vicinity of all of the singular points, $\psi = 0, 1, \infty$, which are $z_O = 0$, $z_C = 0$ and $z_M = 0$. We obtain the transition matrices to connect the three convergence regions by taking sample points that lay at the intersection of the convergence regions of the orbifold-conifold and conifold-LCS and orbifold-LCS. These are shown in Appendix A. Changes of variables from (2.37), (2.36) and (2.35) are made to express the periods in the integral symplectic basis of [32] given in (2.9). The periods in this integral symplectic basis for the three coordinates patches Π_C, Π_M and Π_O are given in formulae (A.5) (A.7) and (A.6) respectively. These explicit formulae in the three different variables allow us to determine the periods, and therefore the scalar potential, in the full CS moduli space up to an arbitrary order.

In the integral symplectic basis the period near the conifold $\Pi_{C,3}$ can be expressed as

$$\Pi_{C,3} = -\frac{1}{2\pi i} \Pi_{C,1} \ln z_C + Q(z_C), \quad (2.38)$$

where $Q(z)$ is a power series in z . This can be seen from (A.5). From (2.38) one reads the monodromy around the conifold which is given by

$$\mu_C = \begin{pmatrix} 1 & 0 & 0 & 0 \\ 0 & 1 & 0 & 0 \\ -1 & 0 & 1 & 0 \\ 0 & 0 & 0 & 1 \end{pmatrix}. \quad (2.39)$$

The periods in the integral symplectic basis in the LCS- and orbifold convergence regions are given to first orders in (A.7) and (A.6). From these expressions one can compute the monodromy matrices around the LCS- and the orbifold point on this basis as

$$\mu_M = \begin{pmatrix} 1 & -1 & 5 & 3 \\ 0 & 1 & -8 & 5 \\ 0 & 0 & 1 & 0 \\ 0 & 0 & 1 & 1 \end{pmatrix}, \quad \mu_O = \begin{pmatrix} 1 & -1 & 5 & 3 \\ 0 & 1 & -8 & 5 \\ -1 & 1 & -4 & 3 \\ 0 & 0 & 1 & 1 \end{pmatrix}. \quad (2.40)$$

The relation between monodromies around the three critical points is given by $\mu_C \cdot \mu_M \cdot \mu_O^{-1} = \mathbb{1}$. In Figure 2 we represent three different paths in CS moduli space giving rise to conifold, LCS and orbifold monodromies.

¹⁰ The LCS monodromy in the basis (2.37) is given by

$$\begin{pmatrix} 1 & 0 & 0 & 0 \\ 2\pi i & 1 & 0 & 0 \\ -10\pi^2 & 10\pi i & 1 & 0 \\ -\frac{20i\pi^3}{3} & -10\pi^2 & 2\pi i & 1 \end{pmatrix}.$$

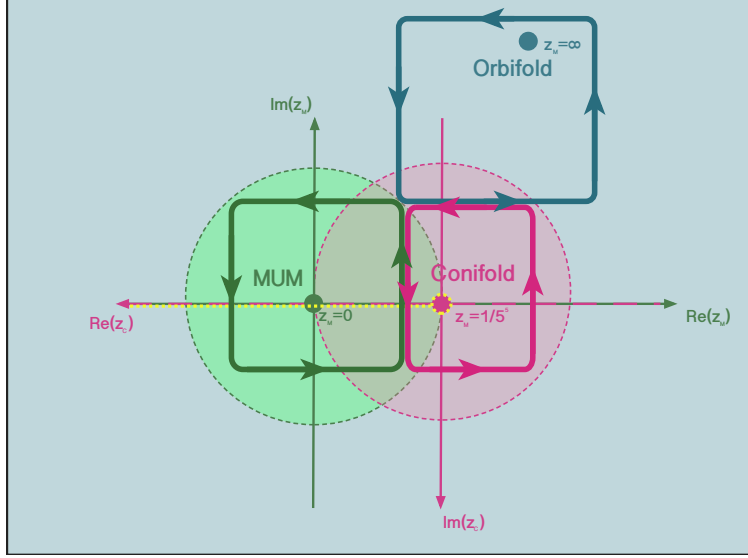


Figure 2: The figure represents three paths leading to monodromies around the critical points of the CS moduli space of the mirror of the quintic CY on \mathbb{P}^4 on the complex z_M -plane. The paths around the LCS, conifold and orbifold points leading to monodromies μ_M , μ_C and μ_O are green, pink and blue respectively.

2.4 Symmetries of the potential

In this section we review the symmetries of the Kähler potential due to transformations of the moduli and how these are broken by the superpotential generated by the fluxes.

First of all, there is a shift symmetry in the real part of the axio-dilation, the 0-form $C_0 \rightarrow C_0 + b$, which is part of the $SL(2, \mathbb{Z})$ symmetry of the theory (see e.g. [45]). Under this shift symmetry, the 3-form flux $G_{(3)}$ remains invariant, which requires $F_{(3)}$ to transform. Therefore, by keeping the fluxes fixed and transforming the axio-dilaton, the shift symmetry is spontaneously broken.

Similarly, there is a shift symmetry in the phase of the complex structure when going around the conifold, $\theta \rightarrow \theta + 2\pi n$ ($z = re^{i\theta}$), with $n \in \mathbb{Z}$. This is a monodromy shift given by n powers of μ_C in (2.39) under which the period Π_3 transforms as

$$\Pi_3 \rightarrow \Pi_3 - n \Pi_1, \quad (2.41)$$

while the Kähler potential (2.7) remains invariant since $\mu_C^T \Sigma \mu_C = \Sigma$. On the other hand, it is easy to check that the superpotential transforms as

$$W \rightarrow W - n G_1 \Pi_1. \quad (2.42)$$

If we also transform the fluxes as (recall that the subindices here denote the component of the flux vector, (2.1))

$$G_3 \rightarrow G_3 - n G_1, \quad (2.43)$$

the superpotential remains invariant. Therefore, by keeping the fluxes fixed, this shift symmetry is spontaneously broken. This is interesting for cosmological applications since a common strategy in the literature in order to find inflation in supergravity and field theory is to consider mildly breaking a symmetry. Indeed, from the discussion above, it is natural to think that either θ or C_0 or a linear combination of these fields, is a good inflaton candidate, which can give rise to either natural or power law types of inflation. This has been the reasoning followed in [18, 25, 27, 28, 31].

Monodromies arising from surrounding the LCS and orbifold point in the CS moduli space, given by (2.40), are also symmetries of the Kähler potential. This is because the monodromies keep the symplectic properties of the period basis i.e. $\mu_{M,O}^T \Sigma \mu_{M,O} = \Sigma$. Again, the superpotential transforms under n monodromies around the LCS or the orbifold, as $W \rightarrow G \Sigma \mu_{M,O}^n \Pi$. This implies that the fluxes have to transform as $G \rightarrow G(\mu_{M,O}^{-1,T})^n$ in order to keep the superpotential invariant. Keeping the fluxes fixed, the symmetries arising from monodromies are spontaneously broken.

Note that since the fluxes are integers, the symmetry breaking will in general be hard to fine tune, unless one also fine tunes the vevs of the other moduli. We will come back to the points discussed here in Section 3.3.

3 Mirror quintic flux vacua: hierarchies and inflation

We have now all ingredients to study the structure of no-scale vacua of the mirror quintic in \mathbb{P}^4 and their potential applications for inflation. We start by revisiting the vacua near the conifold point previously studied in the literature, giving hierarchies among the spacetime- and compactification physical scales in the warped geometry. We then describe our search for vacua using the exact periods and describe their properties and differences with respect to vacua found using only the leading term in the series expansion. We finalise this section with the exploration of slow-roll inflation in this model.

As we saw in Section 2.1, the $\mathcal{N} = 1$ supergravity Kähler potential and superpotential for the dilaton and the complex structure modulus of the mirror quintic are given by

$$K = -\ln[-i(\tau - \bar{\tau})] - \ln[-i \bar{\Pi}^T \Sigma \Pi] , \quad W = G \Sigma \Pi , \quad (3.1)$$

with $G = F - \tau H$, so that the scalar potential is

$$V = \frac{1}{2\kappa_{10}^2 g_s} e^K \left[K^{i\bar{j}} D_i W \bar{D}_{\bar{j}} \bar{W} \right] , \quad (3.2)$$

with $i = \tau, z$ and recall that $\Pi(z)$ are the periods given in the Appendix A. We now look for non-supersymmetric Minkowski vacua of (3.2) with $D_\tau W = D_z W = 0$ and $W \neq 0$. The condition $D_\tau W = 0$ gives an expression for τ in terms of the complex structure modulus as

$$\tau_\tau(z) = \frac{F \Sigma \bar{\Pi}}{H \Sigma \bar{\Pi}} , \quad (3.3)$$

fixing τ as a function of z . Alternatively, one can find $\tau(z)$ from the condition $D_z W = 0$:

$$\tau_z(z) = \frac{F\Sigma(\tilde{\Pi}\Sigma\bar{\Pi})}{H\Sigma(\tilde{\Pi}\Sigma\bar{\Pi})}, \quad (3.4)$$

with $\tilde{\Pi} = \partial_z \Pi \otimes \Pi - \Pi \otimes \partial_z \Pi$ (observe that $\tilde{\Pi}$ has two indices). The subindices τ and z in (3.3) and (3.4) indicate that $\tau_\tau(z)$ and $\tau_z(z)$ are the axio-dilaton profiles obtained from $D_\tau W = 0$ and $D_z W = 0$ respectively. Equating both expressions $\tau_z = \tau_\tau$ fixes the complex structure $z = z_0$, for which the fluxes are constrained to satisfy the well-known condition $*G_3 = -iG_3$. When there is a solution, this is located at $\tau(z_0) = \tau_0$ and $z = z_0$, and it is a Minkowski non-supersymmetric vacuum¹¹ with $V = 0$ provided $W \neq 0$.

A strategy to find Minkowski vacua consists of setting the real and imaginary parts of $\tau_\tau - \tau_z$ to zero. For our numerical analysis, it is convenient to work only with the numerator of this quantity. This allows us to avoid fractional values of polynomials in z and $\ln z$ appearing in $D_z W$ and $D_\tau W$. The numerator of $\tau_\tau - \tau_z$ is given by

$$A_0 = (H\Sigma\bar{\Pi})(F\Sigma(\tilde{\Pi}\Sigma\bar{\Pi})) - (F\Sigma\bar{\Pi})(H\Sigma(\tilde{\Pi}\Sigma\bar{\Pi})). \quad (3.5)$$

With the purpose of finding different Minkowski vacua configurations, we also perform conifold monodromies on the complex structure phase, for which the Kähler potential is invariant, but as already mentioned, this symmetry is broken by the superpotential due to the fluxes. Specifically the period Π_3 in the conifold basis transforms under a conifold monodromy as in (2.41), and since the superpotential transforms as in (2.42), the scalar potential changes as well. Therefore, new vacua can be found by transforming (3.5) under n conifold monodromies changing the periods via $\Pi \rightarrow \mu_C^n \Pi$. The new expression for the numerator of $(\tau_z - \tau_\tau)$ reads

$$A_n = (H\Sigma\mu_C^n \bar{\Pi})(F\Sigma(\mu_C^n \tilde{\Pi}\Sigma\bar{\Pi})) - (F\Sigma\mu_C^n \bar{\Pi})(H\Sigma(\mu_C^n \tilde{\Pi}\Sigma\bar{\Pi})). \quad (3.6)$$

In the next section we use A_n to search for vacua and inflationary regions of the potential.

3.1 Hierarchies revisited

The structure of the vacua for a flux configuration where the only non-vanishing flux components are F_1, H_3 and H_4 , with $H_3 \gg H_4$ in a type IIB CY orientifold compactification, was found in [1]. That study was performed at leading order in the periods series expansion near the conifold point in the CS moduli space. Here we analyse this family of solutions by taking into account higher order terms in the period series. First, we explore modifications to the zeroth order hierarchy expression of [1], coming from constant contributions to $D_z W$. We then search for the exact vacua using the power series of the periods up to convergence order and compare these vacua with the

¹¹Recall again that the Kähler moduli are at this point not stabilised, but we are interested in the dynamics of the dilation and complex structure.

approximations of [1]. Next we review the near conifold vacua solution of [2], and compare it with our exact vacua solutions.

The warped metric which preserves Poincaré symmetry reads [1]

$$ds_{10}^2 = e^{2A(y)} \eta_{\mu\nu} dx_\mu dx_\nu + e^{-2A(y)} \tilde{g}_{mn} dy^m dy^n. \quad (3.7)$$

The hierarchy between the spacetime (4D) and compactification (6D) physical scales will be given by the distance of the vacuum z_0 to the conifold as $e^A \sim z_0^{1/3}$ [1, 46]. In the following we write for our case the solution for z_0 and τ_0 when only the fluxes F_1, H_3 and H_4 are on and $H_3 \gg H_4$. The superpotential (2.16) for this case in terms of $\Pi_C(z_C)$ is given by

$$W = F_1 \Pi_3 + \tau (H_3 \Pi_1 + H_4 \Pi_2). \quad (3.8)$$

The periods were denoted by Π_i instead of $\Pi_{C,i}$, in the rest of this section we adopt this simplified notation, also z_C will be denoted by z . The value of the axio-dilaton arising from the condition $D_\tau W = 0$ is

$$\tau_0 = -\frac{F_1 \bar{\Pi}_3^0}{H_4 \bar{\Pi}_2^0}, \quad (3.9)$$

where $\Pi_i^0 = \lim_{z \rightarrow 0} \Pi_i$ and $\partial_z \Pi_i^0 = \lim_{z \rightarrow 0} \partial_z \Pi_i$ and $z = 0$ is the conifold point. The third period component in the conifold convergence region, given in (A.5), reads $\Pi_3 = \Pi_3^0 + \alpha z + \beta z \ln z + O(z)$. To estimate the complex structure value at the minimum, z_0 , we consider the leading terms in $D_z W = 0$. Let us first note that the derivative of $\partial_z W$ evaluated at (3.9) is given by

$$\begin{aligned} \partial_z W|_{z=z_0} &= F_1 \partial_z \Pi_3 - \frac{F_1 \bar{\Pi}_3^0}{H_4 \bar{\Pi}_2^0} (H_3 \partial_z \Pi_1^0 + H_4 \partial_z \Pi_2^0), \\ &= F_1 (\alpha + \beta + \beta \ln z) - \frac{F_1 \bar{\Pi}_3^0}{H_4 \bar{\Pi}_2^0} (H_3 \partial_z \Pi_1^0 + H_4 \partial_z \Pi_2^0) + O(z). \end{aligned} \quad (3.10)$$

The covariant derivative then reads

$$\begin{aligned} D_z W &= \partial_z W + \partial_z K_0 W_0 + O(z), \\ &= F_1 \beta \ln z + \tau_0 H_3 \partial_z \Pi_1^0 + a_0 + O(z), \end{aligned} \quad (3.11)$$

where

$$\begin{aligned} W_0 &= (F_1 \Pi_3^0 + \tau_0 (H_3 \Pi_1^0 + H_4 \Pi_2^0)), \\ \partial_z K_0 &= -(\bar{\Pi}_2^0 \partial_z \Pi_4^0 - \bar{\Pi}_4^0 \partial_z \Pi_2^0 - \bar{\Pi}_3^0 \partial_z \Pi_1^0) / (\bar{\Pi}_2^0 \Pi_4^0 - \bar{\Pi}_4^0 \Pi_2^0), \\ a_0 &= F_1 (\alpha + \beta) + \tau_0 H_4 \partial_z \Pi_2^0 + \partial_z K_0 W_0. \end{aligned} \quad (3.12)$$

We use these relations to define a parameter δ_0 , which will allow us to measure the departure from our result to that in [1], as:

$$\delta_0 = \frac{a_0}{F_1} = \alpha + \beta - \frac{\bar{\Pi}_3^0}{\bar{\Pi}_2^0} \partial_z \Pi_2^0 + \partial_z K_0 \Pi_3^0 - \partial_z K_0 \frac{\bar{\Pi}_3^3}{\bar{\Pi}_2^0} \Pi_2^0,$$

where we used (3.9) and W_0 in (3.12).

Substituting the value of Π_1 at the conifold point, $\Pi_1^0 = 0$, neglecting $O(z)$ and for the moment, δ_0 terms (which are $O\left(\frac{H_3}{H_4}\right)$) one gets¹²

$$z_{old} = \exp\left(\frac{H_3}{H_4} \frac{\partial_z \Pi_1^0 \bar{\Pi}_3^0}{\beta \bar{\Pi}_2^0}\right) = \exp\left(-\tau_0 \frac{H_3}{F_1} \frac{\partial_z \Pi_1^0}{\beta}\right). \quad (3.13)$$

This is the result obtained in [1], written in our notation. Let us now see how this result changes when we include the corrections due to the parameter δ_0 . When we take into account this correction, (3.13) becomes

$$z_{new} = \exp\left(\frac{H_3}{H_4} \frac{\partial_z \Pi_1^0 \bar{\Pi}_3^0}{\beta \bar{\Pi}_2^0} - \frac{\delta_0}{\beta}\right). \quad (3.14)$$

Therefore we see that there is an extra factor $\exp\left(-\frac{\delta_0}{\beta}\right) \sim 20$, due to the neglected terms contributing to $D_z W = 0$. Using the expressions above, we can now check the effects of the corrections due to δ_0 . We show this in Figure 3. We compare first the full value of τ_0 (3.9) at the minimum as a function of H_3 (the two plots in the first line) with respect to the approximated value obtained in [1], which corresponds to the constant red line in the plots. As can be seen, τ_0 converges rapidly to the approximated value at the minimum as the flux is increased. Notice also that a small perturbative value of g_s depends on the smallness of the ratio F_1/H_4 . Next we do the same for $|z_0|$ (first plot in the second row). Here it is clear that the approximated value (dotted orange line) for $|z_0|$ does not converge to the actual value (blue continuous line) even when the flux increases. In the last two pictures we plot instead the true value at the vacuum (the dots) and the δ_0 corrected value z_{new} (orange continuous line). The convergence is almost instantaneous. Therefore, we see that the estimated value for $|z_0|$ is better represented by our corrected expression (3.14). In Appendix B we write the correction (3.14) in the notation of [1].

More generic flux configurations

We now give a condition for general configurations of fluxes that can be used for finding vacua with hierarchies. In doing this, the fluxes F_3 and H_3 play an important role, because it is possible to leave the value of the axio-dilaton fixed, by varying these fluxes, as was done in [1] for H_3 . The solution for z_0 , with $|z_0| \ll 1$ at the minimum for arbitrary fluxes was given in [2] and there it was also found that the density of vacua near the conifold is high. Here we will see how varying F_3 and H_3 , one can move close to the conifold point and that the true vacua approach to z_0 only if the condition $|z_0| \ll 1$ is satisfied.

¹²The derivative of K reads $\partial_z K = -\frac{\bar{\Pi}^T \Sigma \partial_z \Pi}{\bar{\Pi}^T \Sigma \Pi}$, and closed to the conifold its more relevant contribution would come from $\bar{\Pi}_1 \partial_z \Pi_3 \sim \bar{\Pi}_1^0 \beta \ln z$, but $\bar{\Pi}_1^0 = 0$. Therefore the most relevant contribution is the constant term $\partial_z K_0$.

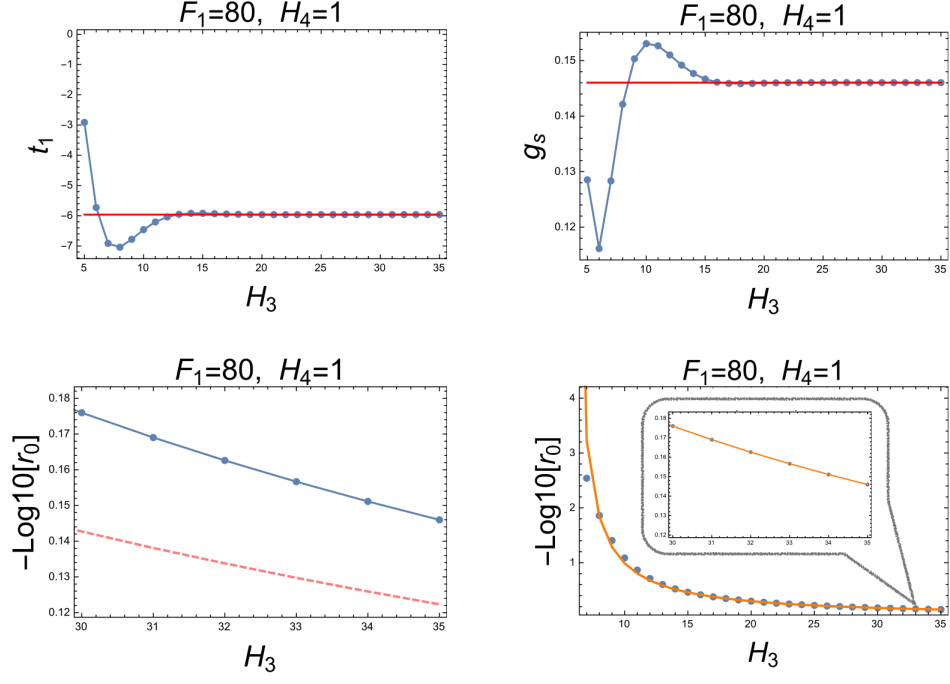


Figure 3: The plots on the first row show t_1 and g_s vacua true values (dots) for the set of fluxes $F_1 = 80, H_4 = 1$ and variable H_3 , with the red line representing the hierarchical solution of [1]. First plot on the second row represents the absolute value of $|z_{old}|$ (3.13) for the solution of [1] (dashed line) compared with the true vacua solutions $|z_0|$ (dots). Second plot on that row represents $|z_{new}|$, the corrected equation (3.14) (yellow line) compared with the true vacuum $|z_0|$ (dots).

Let us first find the approximate value of z_0 for a vacuum near the conifold point. The covariant derivative $D_z W$ close to the conifold point to leading order reads

$$D_z W = (F_1 - \tau_0 H_1) \beta \ln z + (F_1 - \tau_0 H_1)(\alpha + \beta) + (F_2 - \tau_0 H_2) \partial_z \Pi_4^0 - (F_3 - \tau_0 H_3) \partial_z \Pi_1^0 - (F_4 - \tau_0 H_4) \partial_z \Pi_2^0 + \partial_z K_0 W_0, \quad (3.15)$$

where

$$\tau_0 = \frac{F \Sigma \bar{\Pi}^0}{H \Sigma \bar{\Pi}^0}, \quad W_0 = (F - \tau_0 H) \Sigma \Pi^0. \quad (3.16)$$

(Note that τ_0 here depends on the fluxes). This gives as a solution for z_0 :

$$z_0 \sim \exp \left(- \left(\frac{\alpha}{\beta} + 1 \right) + \frac{-(F_2 - \tau_0 H_2) \partial_z \Pi_4^0 + (F_3 - \tau_0 H_3) \partial_z \Pi_1^0 + (F_4 - \tau_0 H_4) \partial_z \Pi_2^0 - \partial_z K_0 W_0}{\beta (F_1 - \tau_0 H_1)} \right). \quad (3.17)$$

Now, since $\Pi_1^0 = 0$ the contribution of the fluxes F_3 and H_3 in τ_0 is absent and therefore we can tune these to achieve a small $|z_0|$, which gives hierarchies, while preserving a stabilised perturbative $g_s < 1$. We show this explicitly in Figure 4 for two configurations of fluxes. We compare the approximate value of z_0 given by (3.17) and its real value using the exact periods¹³. The figures show that the calculation with the period expansion and the approximation (3.17) differ on a $\sim 1\%$ for $|z_0| \sim 10^{-1}$. However even for points inside the conifold convergence region, the difference is higher, for example for $|z_0| \sim 0.5$ the difference is a $\sim 12\%$.

3.2 Search for vacua

We search for Minkowski vacua for different flux configurations. Since we are looking for vacua numerically, the solutions will depend on the approximation taken for the expansions of the periods. Through our explorations we explore the convergence of r up to order 600 in the expansions. From our search we identify different generic properties of the vacua depending on our choice of fluxes, conifold monodromies and location with respect to the critical points. These are as follows:

1. We find Minkowski vacua for which the complex structure axion value lies outside the basic domain region from 0 to 2π . We did not find inflationary regions for models allowing these vacua. See Section 3.3.
2. We find *Fake* Minkowski vacua, for which all moduli vevs depend on the order of the approximation on the period series.

¹³Where by exact we mean that we employ as many necessary terms in the period series so as to achieve convergence, as already mentioned.

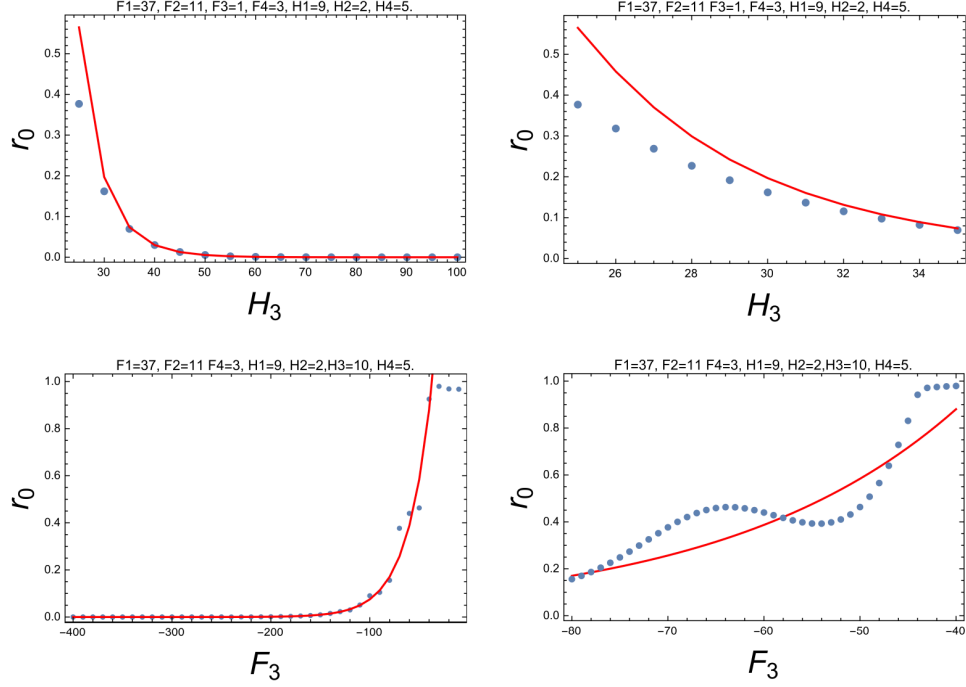


Figure 4: The first plot shows the exact $|z_0|$ for vacua solutions vs. H_3 (blue dots) together with approximation (3.17) (red line). The second plot is a zoom of the first, showing more clearly the difference between the exact solution and the approximation. The third and fourth plots show the exact vacua solutions (dots) and the approximation (3.17) vs. F_3 , and its zoom. Turning on H_3 and F_3 , leaves g_s fixed and leads to vacua close to the conifold. This implies a hierarchy between the four and six dimensional scales.

3. Inflationary regions are present for small and “large” values of the distance to the conifold $r = |z_0|$. This was checked starting with a given order in the series expansion, and holds for an arbitrary order. No Minkowski vacua were found for the choices of fluxes in these cases. In one case we found a de Sitter vacuum. We discuss this in Section 3.3.

In all solutions, the values of the fluxes can be tuned to achieve a perturbative value of g_s , $g_s < 1$. We now discuss these cases in more detail.

I. Minkowski vacua

We present here the flux configurations for which there are stable Minkowski vacua in a region close to the conifold point ($r < 1$). Some generic features about these solutions are the following:

- We found several Minkowski exact vacua within the conifold convergence region using the period series expansion $\Pi_C(z_C)$ in (A.5). The order in the period’s series expansion is increased up to achieve convergence. In some cases we stopped at order 200, but we have obtained the period series up to order 600. In Table 3.1 we present 14 of these vacua.

	r	θ	t_1	t_2	(F_1, H_1)	(F_2, H_2)	(F_3, H_3)	(F_4, H_4)
1	0.00387722	-7.01112	-2.965416	3.421883	(40,0)	(0,0)	(0,16)	(0,1)
2	0.289795	-3.90606	-7.0416876	7.0353577	(80,0)	(0,0)	(0,8)	(0,1)
3	0.289795	-3.90606	-176.04219	175.88394	(2000,0)	(0,0)	(0,8)	(0,1)
4	0.289795	-3.90606	-4.40105	4.3971	(50,0)	(0,0)	(0,8)	(0,1)
5	0.476018	-21.5600	-3.54466	5.02946	(9*10,1)	(0,0)	(27*10,16)	(0,2)
6	0.26791	-2.65769	-1.13736	2.11955	(20,0)	(0,0)	(0,8)	(0,1)
7	0.0038772	-7.01111	-4.44813	5.13282	(60,0)	(0,0)	(0,16)	(0,1)
8	0.0553517	-1.88428	-5.51566	20.8484	(200,1)	(30,1)	(2,10)	(2,1)
9	$2.07602 \cdot 10^{-6}$	-13.6039	-5.96259	6.84777	(80,0)	(0,0)	(0,30)	(0,1)
10	0.160500	1.7234	0.407671	0.81259	(37, 9)	(11, 2)	(1, 31)	(3, 5)
11	0.000301	7.2269	-1.22438	44.711	(16, 2)	(7, 7)	(1, -8)	(4, -1)
12	$6.28576 \cdot 10^{-8}$	-4.06	123.57	124.58	(36, 2)	(107, 0)	(0, 5)	(0, 1)
13	$8.91875 \cdot 10^{-7}$	-47.91	-4.75	1.56681	(2, 0)	(4, -2)	(1, 3)	(1, 0)
14	0.03351	6.28319	-3	3.71019	(3, -1)	(3, 0)	(1, 1)	(0, 0)

Table 3.1: The table shows the values of the moduli at the minima of the scalar potential V in the conifold convergence region. Solutions for fluxes where H_i and F_i are proportional, have the same z and have values of τ related as in (3.18). Here $z_C = re^{i\theta}$, $\tau = t_1 + it_2$ and the fluxes are given in string units.

- Solutions where the vacuum lies very close to the conifold point present a large hierarchy between the internal and the macroscopic dimensions, confirming the results of [1] up to the correction (3.14). These were found considering only the leading contribution to the periods

and non-zero $F_1, H_3, H_4 \neq 0$, $H_3 \gg H_4$. In Figure 3 we compare the value of z_0 with the one of the convergent solution for different values of H_3 with fixed values of F_1 and H_4 . An example is the vacuum 9 in Table 3.1, where $|z_0| \sim 2 \cdot 10^{-9}$. One can slightly deviate from these solutions by turning on nonzero values of H_1 or F_3 . Also the vacua on Table 3.1 with more generic flux configuration possessing hierarchies are obtained by the guideline of considering $|z_0| \ll 1$ in (3.17), examples of vacua with a strong hierarchy are 12 and 13 in the table.

- For a specific flux configuration with only F_1 and H_3 non-zero it is straightforward to see from eq. (3.5) that the solution for z does not depend on the fluxes. Hence, if there is a z_0 vacuum solution, this is unique for all set of fluxes (F_1, H_3) . However, studying the sample case $H_3 = 16$ and $F_1 = 1$ we find, in agreement with [1], that is not possible to find a vacuum close to the conifold point for this flux configuration, which in turn implies the absence of a solution for any flux configuration of this type. We have checked this using an expansion for the periods around the conifold up to order 200. A simpler argument tells that a near to the conifold solution will have the approximate value of $\tau_0 = -\frac{F_1 \Pi_3^0}{H_3 \Pi_1^0} \rightarrow \infty$, since $\Pi_1^0 = 0$.
- Another feature of the solutions comes from the set of equations (3.3) and (3.4), from which one can see that two flux configurations $(F^{(1)}, H^{(1)})$ and $(F^{(2)}, H^{(2)})$ with components related by

$$\frac{F_i^{(1)}}{H_i^{(1)}} = k \frac{F_i^{(2)}}{H_i^{(2)}}, \quad \forall_i \quad \text{with } k \in \mathbf{Q}. \quad (3.18)$$

will have stable vacua at the same value of the complex structure and a fixed dilaton value related by $\tau_0^{(1)} = k\tau_0^{(2)}$. This defines a similarity relation and therefore a characteristic class $[F, H]$ to which all the above fluxes belong to. In terms of the corresponding characteristic class, there is only a single vacuum.

- To check the solutions found in the conifold convergence region in terms of Π_C we explore them also on other patches (LCS, orbifold, regular point). This is particularly relevant for vacua that are apparently located close to the boundary of the conifold convergence region, using instead of Π_C periods's expansions that converge faster to the solution. The periods expanded in local coordinates near a critical point have the corresponding monodromy automatically. For example the Π_C expansion has the term $\ln z_C$, causing the monodromy μ_C that is absent in Π_O and Π_M . If the periods are expressed as local series expansion in the variables of other patches, the monodromy around the original critical point has to be implemented by hand. We find Minkowski vacua as zeroes of the numerator of $(\tau_z - \tau_\tau)$, which transforms under monodromies μ_C as in formula (3.6). Vacua exploration on patches different from z_C corresponds to finding zeroes of it. The periods written as a series of the complex structure modulus in the three different coordinate systems z_C, z_M and z_O are given in Appendix A.

- We found that the monodromies play an important role in finding vacua. For certain sets of fluxes, the region $0 \leq \theta < 2\pi$ does not contain Minkowski vacua, and one can only satisfy the conditions $V = \partial_i V = 0$ after taking monodromies around the conifold point, starting from that domain. This can be seen in Table 3.1. The vacua presented there are only found for a given value of θ but they vanish when taking $\theta \rightarrow \theta + 2\pi n$, $n \in \mathbb{Z}$. However, for certain configurations of fluxes, it is possible to find vacua at every monodromy turn differing in the values of the other moduli [2].

For all the reported vacua, the corresponding mass matrix is positive definite ensuring stability of the minima (up to Kähler moduli).

II. Fake Minkowski vacua

Our study shows that in order to find true vacua and study their properties, it is necessary to include higher order terms in the series expansion of the periods in terms of the complex structure modulus. Staying at leading order leads to vacua which vanish when higher order terms are taken into account. Let us give an example of this: in Figure 5, we plot the value of $|z_0|$ for two different sets of fluxes. The first has an apparent vacuum at leading order in the series expansion. However, as higher orders are included, the apparent vacuum solution does not converge to a final value. Additionally the root approaches to the boundary of convergence. In the figure we see that convergence is not reached even after taking 200 orders in the series; the $n + 1$ value differs from the n values by about 1%. We checked in the orbifold patch for this vacuum and it is absent, which tells us that it is an error of the approximation. On the right picture we see a second configuration of fluxes for which the vacuum solution at the leading order, remains practically unchanged after the 200th order. Indeed, in this case, convergence to the actual vacuum is achieved very quickly.

3.3 Inflationary regions

In this section we explore the *full* complex structure moduli space in order to determine whether inflationary directions can generically appear in the scalar potential. The CS moduli space has been explored in several papers in the literature. In [18, 27, 25], axion inflation was studied in the small region of the moduli space near the LCS point at leading order in the periods' expansion, while in [31] scalar potentials near the critical points were explored at leading order in the period's series expansion. The recent work of [28] on the other hand, studied the scalar potential in the region close to the LCS point, but considered only a small number of terms in the series' expansion. We will comment further on this work below. A standard strategy to look for potential inflationary directions in the literature, is to track symmetries of the Kähler potential, which may be slightly broken by some effect, such as fluxes. In Section 2.4, we discussed the symmetries of the Kähler potential when transforming the dilaton and the phase of the complex structure moduli, in particular

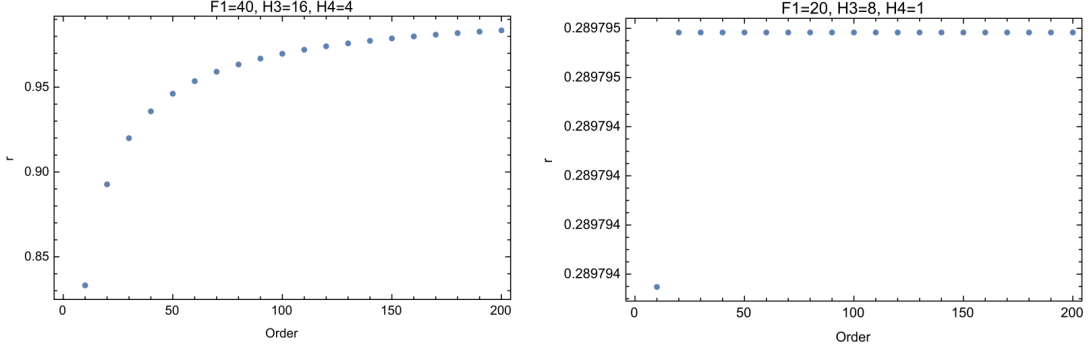


Figure 5: Vacuum solutions vs. the order in the period expansion for two sets of non-zero fluxes. The vacuum solution on the left does not converge inside the conifold convergence region after order 200th, and thus does not correspond to a true vacuum. Instead, the solution on the right converges very quickly to a stable value.

by a shift. Following this line of thought, we first let the fields evolve and look for regions in the moduli space where the generalised slow roll conditions for multi-field inflation are satisfied mostly along the axionic directions: the complex structure phase θ and $\text{Re}(\tau)$. The multi-field slow-roll parameters are given by (see e.g. [47]):

$$\epsilon = M_{Pl}^2 \frac{K^{i\bar{j}} \nabla_i V \nabla_{\bar{j}} V}{V^2}, \quad \eta = \min \text{ eigenvector} \left[\frac{K^{i\bar{j}} \nabla_i \nabla_{\bar{j}} V}{V} \right], \quad (3.19)$$

where ∇ is the covariant derivative in the moduli space.

Using this approach, we did not find field regions where θ and $\text{Re}(\tau)$ have long displacements and slow-roll parameters are small. This check was done at an arbitrary order in the series expansion of the periods. This can be understood in the following way. From the form of K and W , considering all fields but θ fixed, it is easy to see that, due to the presence of the logarithms in the periods, the scalar potential will contain powers of θ , besides sines and cosines, giving

$$V(\theta) \sim A + B \theta^2 + C \theta \cos \theta + \dots \quad (3.20)$$

where A, B depend on the other moduli and the fluxes, and the dots include further mixed terms, including sines and cosines multiplied by powers of θ . This rather generic form of the potential for the complex structure axion was pointed out in [28]. However, while in [28] it is argued that this kind of potential can give rise to natural inflation, in several cases we find that the modulations of the potential along the θ -direction, are too high to allow for slow roll inflation. Moreover the amplitude of the oscillations increases with $|\theta|$ (see Figs. 6 and 7). However, as pointed out in [48], it is possible that more general slow-roll regions appear in this direction, allowing for inflation. We also calculated ϵ assuming single-field inflation along the θ direction, keeping all other moduli fixed. We found that in some cases it was possible to get $\epsilon \ll 1$, however the r direction was highly

unstable, and therefore the multi-field ϵ differed very much from the single field approximation. This can be understood as due to higher order corrections in the period series giving contributions to the potential producing interaction terms between r and θ .

Given this result, we explored the scalar potential in all possible directions. We searched systematically for numerical minimisation of ϵ , varying z , τ and the fluxes, subject to constraints on z_0 and τ_0 on (3.17)(3.16), $|z_0| \ll 1$ and $\text{Im}(\tau_0) > 1$ respectively. We found no flux configuration where a Minkowski vacuum near the conifold and $\epsilon \ll 1$ occurs simultaneously. Discarding the restriction of having a vacuum near the conifold point, we found through numerical minimisation, small values of ϵ for certain regions of z, τ and flux configurations. For those cases there were no Minkowski vacua found on the orbifold and LCS convergence regions. We discuss below our results.

1. We found that for configurations of fluxes with a Minkowski vacuum, there are no regions where the multi-field slow roll parameters (3.19) are smaller than one. This is shown in Figure 6, where there were no inflationary regions (defined as regions with $\epsilon, \eta < 1$). Again, it is possible that we miss more general slow-roll regions as discussed recently in [48]. Indeed, the potential along the θ direction shown in Figure 6 resembles closely those discussed in [48].
2. We found configurations of fluxes (see Table (3.2)) for which large inflationary regions are present. We show examples of this in Figures 9-11. As in the previous case, large modulations appear due to higher order terms in the series expansion. We show this in Figure 7 where we also show the difference among modulations for the potential as function of θ only, when the first and fourth order terms are kept. In Figure 8 we illustrate the effect of taking into account higher order terms in the series expansion of the periods, by plotting the values of ϵ at different points in the moduli space vs. the order of the expansion.

These configurations of fluxes however, did not give rise to Minkowski vacua since the equations $D_\tau W = D_z W = 0$, did not have a solution. In the conifold convergence region this happens because the solutions to both constraints τ_τ and τ_z on (3.3) and (3.4) give imaginary parts with opposite signs. Interestingly, for these configurations we found many saddle points with a generic feature: the main unstables direction are given by θ and r . Given this observation, we explored inflationary regions near the orbifold singularity as we discuss below. The precise location of saddle points turns out to be highly affected by the order of the series expansion, but convergence is obtained. Additionally we found a dS vacuum for a flux configuration satisfying slow-roll conditions. This case is presented in Figure 10. This solution is interesting as it may give an explicit realisation of the uplift mechanism proposed in [49] once we include the Kähler moduli.

In Figures 9, 10, 11 and 12 we show examples of $\epsilon \ll 1$ values for different flux configurations on the conifold convergence region. In Table 3.2 we show those flux configurations and two others where also $\epsilon \ll 1$ values were found. In all of the cases the fluxes do not satisfy the condition to encounter a hierarchical vacuum near the conifold ($|z_0| \ll 1$, z_0 in (3.17)).

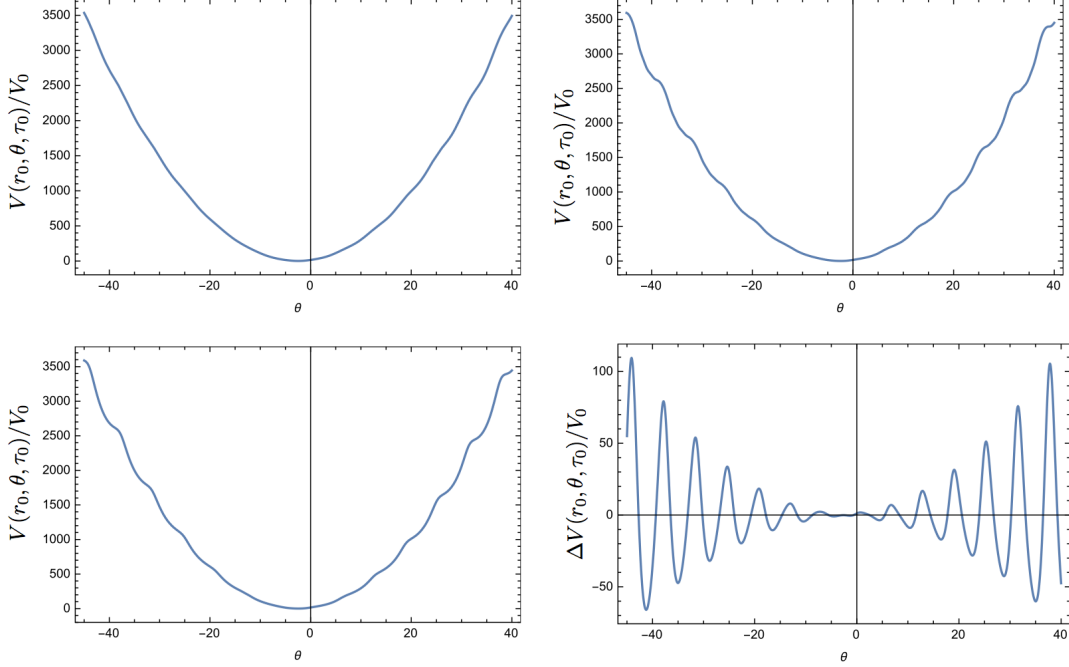


Figure 6: Scalar potential vs. θ and the rest of the moduli fixed at their vev's for a configuration with non-zero fluxes $F_1 = 20$, $H_3 = 8$, $H_4 = 1$ and a Minkowski vacuum. Here $V_0 = \alpha'^2/(2\kappa_{10}^2 g_s)$ and the fluxes are given in string units. The values of the other moduli are set at $r_0 = 0.26791$, $t_1 = -1.13736$, $t_2 = 2.11955$. The figures show the scalar potential approximations to order 1, 4, 200 in z from left to right and up to down. The last plot indicates the difference between order 200 and the order one calculation.

F_1, H_1	F_2, H_2	F_3, H_3	F_4, H_4
1,1	0,-10	0,1	-10,1
2,4	2,4	1,2	3,1
1,3	0,0	10,2	0,1
2,4	0,0	6,2	0,2
43,10	193,64	198,-10	-10,-10
90,3	193,165	-10,0	-10,0

Table 3.2: Configurations of fluxes for which inflationary regions appear, but there are no Minkowski vacua.

The slow-roll conditions found for this type of flux configurations occurred in general in a multifield fashion. For example in Figure 9 the η -eigenvector along the minimum η -eigenvalue (η_{min}) is given mostly in the r direction. On the other hand in Figure 10 and Figure 12 the dominant contributions to the η_{min} eigenvector are given by t_1 and t_2 . Finally in Figure 11 the dominant contribution is given mostly along the direction of t_1 . In Figs. 9-13 we give an estimate of the displacements of the canonical fields $\phi_r, \phi_\theta, \phi_{t_1}, \phi_{t_2}$ defined as

$$\begin{aligned}\partial_\mu \phi_\theta &= M_{Pl} \sqrt{K_{z\bar{z}}} r \partial_\mu \theta, \quad \partial_\mu \phi_r = M_{Pl} \sqrt{K_{z\bar{z}}} \partial_\mu r, \\ \partial_\mu \phi_{t_1} &= M_{Pl} \frac{\partial_\mu t_1}{2t_2}, \quad \partial_\mu \phi_{t_2} = M_{Pl} \frac{\partial_\mu t_2}{2t_2},\end{aligned}$$

in the inflationary region. We evaluate the quantities above locally¹⁴ in order to estimate the displacements of the canonical fields on the slow-roll region.

There seems to be no pattern indicating that slow-roll regions occurs along a preferred direction. In particular it doesn't occur necessarily along a direction with a shift symmetry. For example we did not find flux configurations with slow-roll conditions where θ is the dominant slow-roll direction. This observation indicates that to achieve slow-roll along θ one would require a careful fine tuning of the fluxes, which will be hard to do as they are integers.

3. Finally, we also explored slow-roll conditions on the orbifold convergence region. This exploration is motivated by our findings that the flat directions on the previous cases seem to extend for larger values of r_C , going outside the conifold convergence region with boundary at $r_C = 1$. In Figure 13 we show the density plots of ϵ on six different planes of the moduli space in the orbifold convergence region, for the same flux configuration as in Figure 12. For this configuration there is a saddle point inside the orbifold convergence region. However there are no Minkowski nor dS vacua.

¹⁴By locally here we mean that the values of the other moduli are frozen when defining the canonical field for a single modulus. For example for small field displacements $\delta r, \delta \theta, \delta t_1, \delta t_2$ around the point $r_0, \theta_0, t_{1,0}$ and $t_{2,0}$ the canonical fields are given by $\partial_\mu \phi_{t_1} = \partial_\mu \frac{t_1}{2t_2^0} + O(\delta t_1, \delta t_2)$, $\partial_\mu \phi_{t_2} = \partial_\mu \frac{t_2}{2t_2^0} + O(\delta t_1, \delta t_2)$, $\partial_\mu \phi_r = \partial_\mu (\sqrt{K_{z\bar{z}}^0} r) + O(\delta r, \delta \theta)$, $\partial_\mu \phi_\theta = \partial_\mu (\sqrt{K_{z\bar{z}}^0} r_0 \theta) + O(\delta r, \delta \theta)$.

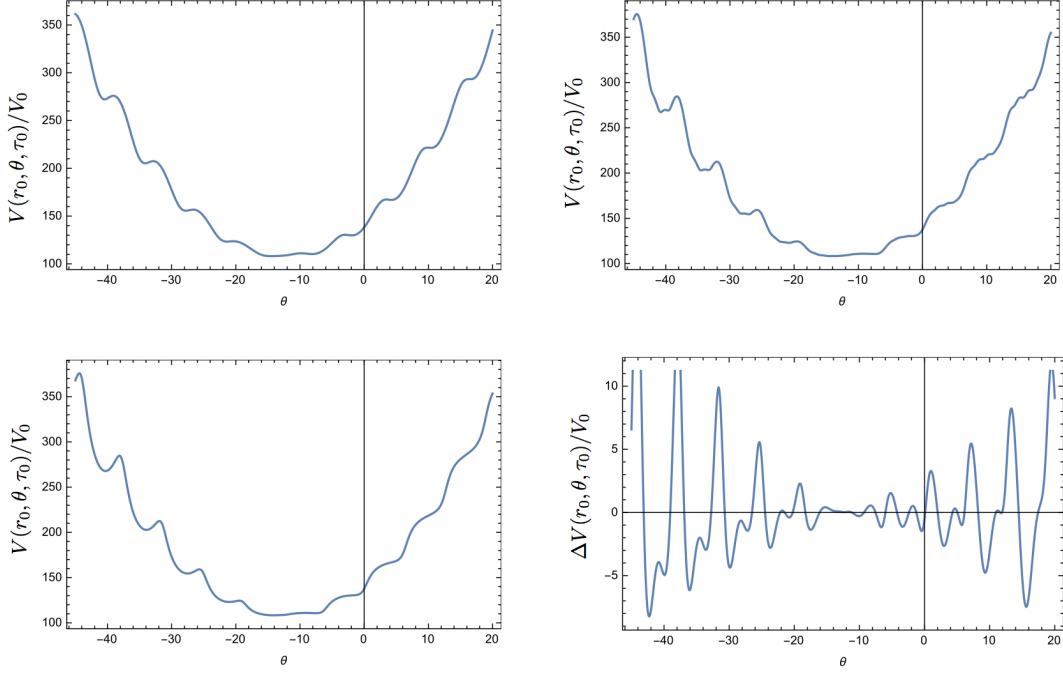


Figure 7: Scalar potential vs. θ and the rest of the moduli fixed at their vev's for a configuration with non-zero fluxes $F_1 = H_1 = 1$, $F_4 = H_2 = -10$, $F_2 = F_3 = 0$, $H_3 = H_4 = 1$ and a Minkowski vacuum. The values for the rest of the moduli are: $t_1 = -6.28$, $t_2 = 16$, $\theta_0 = -12$, $r_0 = 0.4$. The figures show the scalar potential approximations to order 1, 4, 200 in z from left to right and up to down. The last plot indicates the difference between order 200 and the order one calculation. The θ asymmetry arises due to the odd powers of θ multiplying oscillatory functions appearing in the potential. Here again $V_0 = \alpha'^2/(2\kappa_{10}^2 g_s)$ and the fluxes are given in string units.

Note that the distance between critical points of the complex structure moduli space is finite. Therefore the displacements of the canonical field for r , ϕ_r , are bounded in M_{Pl} units. We show this in Figure 14 where we plot the evolution of the locally normalised canonical fields ϕ_r and ϕ_θ vs. the moduli r and θ for the conifold and the orbifold convergence regions.

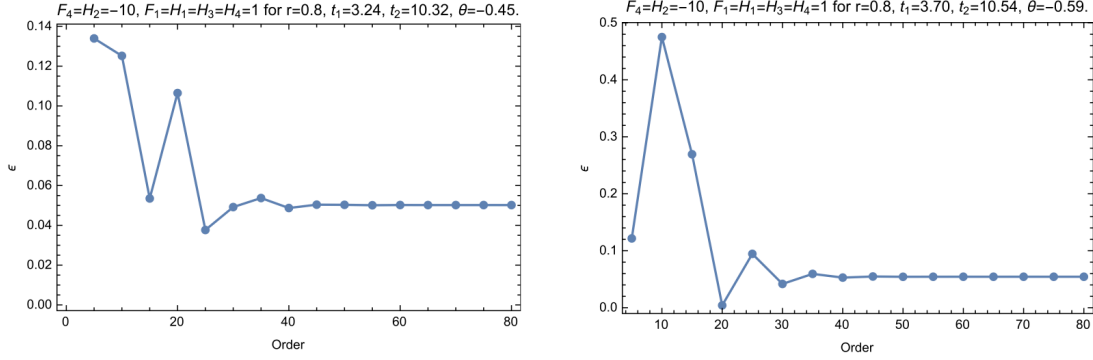


Figure 8: The value of ϵ vs. the order in the periods' series expansion. The fluxes are the same that in Fig.9. The values of the moduli for each case are given above the figures. This shows that ϵ 's convergence is slow as we increase the order in the series expansion. The values of ϵ can differ in a 92% from the order 20 to the order 100. Convergence is achieved: the value of ϵ at order 80 differs from the order 100 by $6 \times 10^{-4}\%$.

4 Conclusions

We explored the moduli space of no-scale type IIB orientifold flux compactification on the mirror quintic Calabi-Yau 3-fold. For the complex structure modulus, we solved the Picard-Fuchs equations in four convergence regions: the orbifold, the conifold, the large complex structure points patches and in a regular point patch. This allowed us to have exact expressions for the periods in the whole complex structure moduli space. The solutions to the PF equations have been previously studied in the literature [33, 38], and we have extended this study in the present work by computing them to all orders in the series required to achieve convergence.

Using these solutions we explored the four dimensional moduli space composed of the complex structure modulus z and the axio-dilaton τ . We searched for Minkowski vacua, vacua with hierarchies and regions with small multi-field slow-roll inflationary parameters ϵ, η (defined in eq. (3.19)). We gave special attention to the periods in the conifold convergence region, where we compared vacua obtained using the series expansion to an arbitrary order approximation with those obtained using an approximation near the conifold point. We found that Minkowski vacua are in general absent in the fundamental domain of $\theta = \arg(z)$, while vacua appear generically when monodromies around the conifold are taken. We pointed out the importance of considering higher order terms in the periods' series expansion in z to ensure the existence of the vacua. Specifically, we found that some Minkowski vacua appearing at leading order near the conifold, disappear when higher order terms in z are considered. These fake vacua turn out to be an effect of the approximation, and by careful analysis in a different patch (in the vicinity of the orbifold, LCS, or a regular point) they can be discarded.

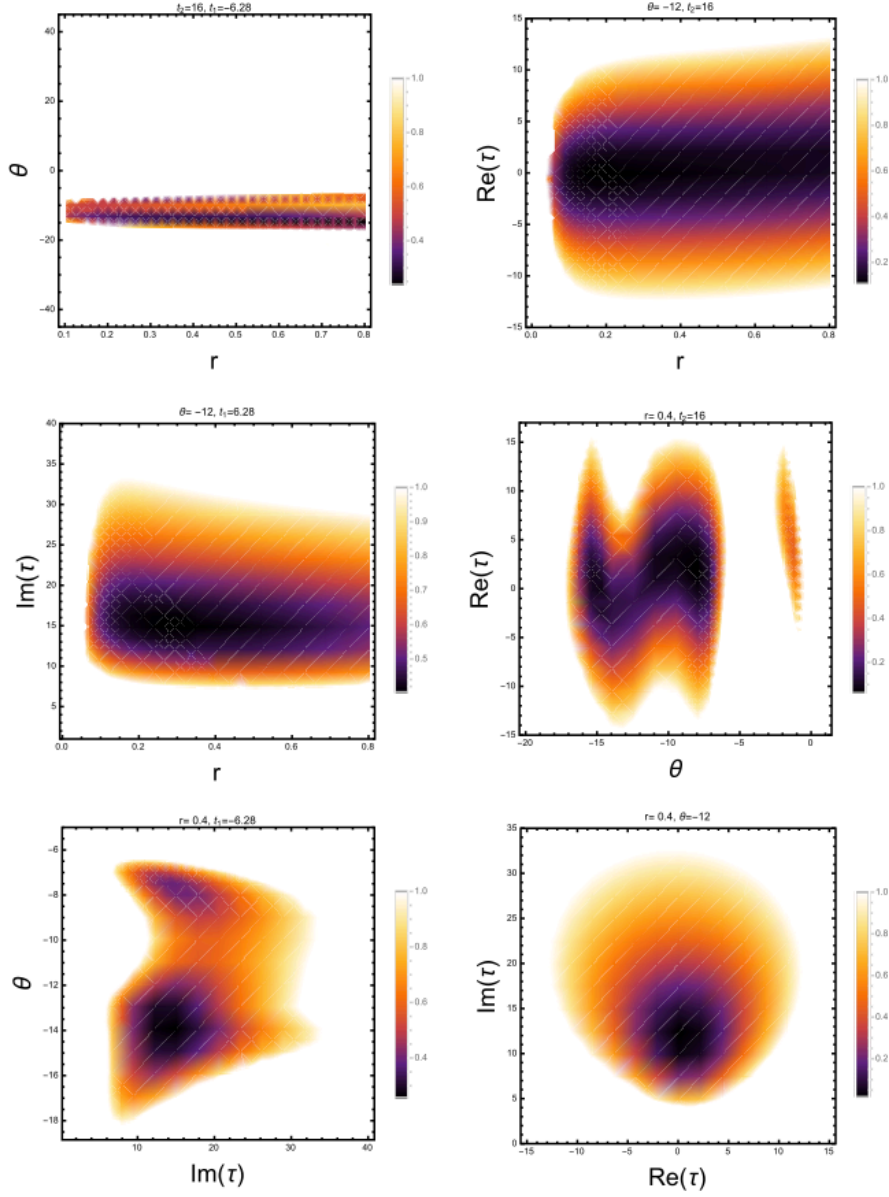


Figure 9: ϵ density plot for the flux configuration $F_1 = H_1 = H_3 = H_4 = 1$, $F_4 = H_2 = -10$, $F_2 = F_3 = 0$. The CS modulus is in the conifold patch $z_C = re^{i\theta}$ and evaluations are performed to order 200 in the period series expansion Π_C . The projections on the different planes are made by fixing the values of the moduli at $t_1 = -6.28, t_2 = 16, r = 0.4, \theta = -12$, respectively. The smaller values of ϵ in this region turned out be of order $\epsilon \sim 0.05$. In this region we also find $\eta < 1$. A sample η eigenvalue is $\eta_{100} \sim -0.07$ for the point $r = 0.37, t_1, \theta$ as before and $t_2 = 9$, corresponding to the eigenvector $\sim (0.12, 0.004, 0.99, 0.09)$, which indicates that the r direction is the dominant one along the inflationary direction. For the canonically normalized fields, the displacements in Planck units on the represented region are of order $\Delta\phi_r \sim 0.1M_{Pl}$, $\Delta\phi_\theta \sim 0.3M_{Pl}$, $\Delta\phi_{t_2} \sim 0.79M_{Pl}$, $\Delta\phi_{t_1} \sim 0.78M_{Pl}$.

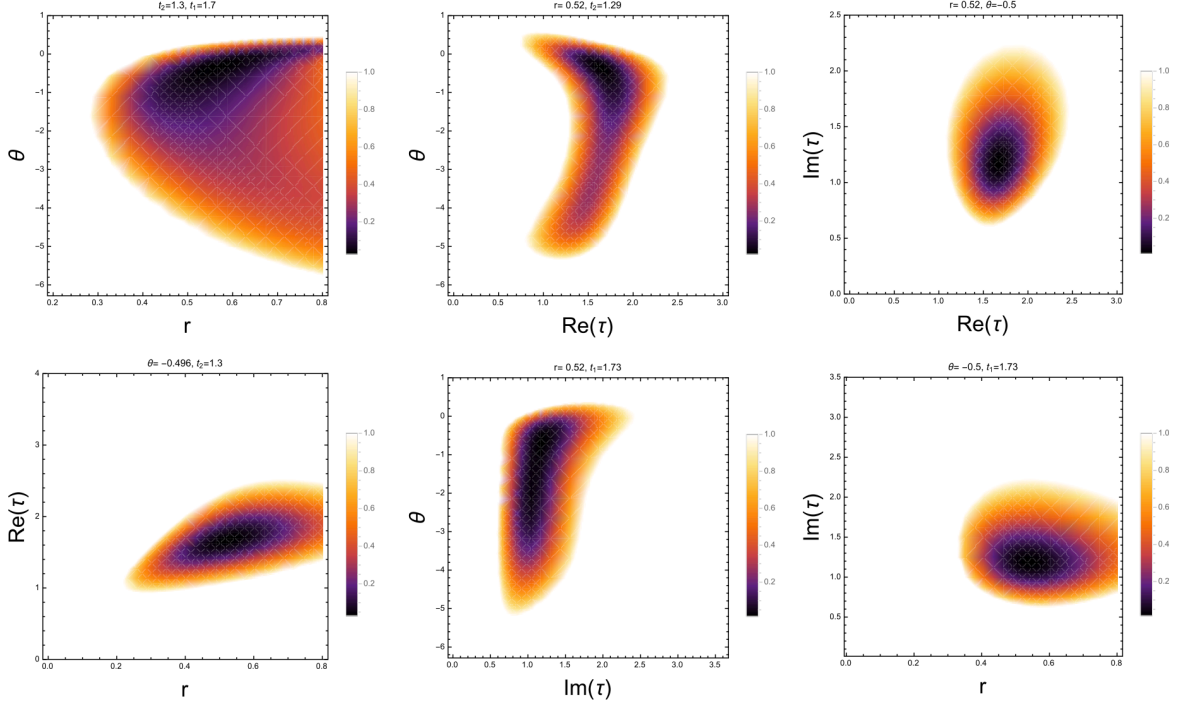


Figure 10: Density plot for ϵ for a configuration of non-zero fluxes $F_1 = 2$, $F_2 = 2$, $F_3 = 1$, $F_4 = 3$, $H_1 = 4$, $H_2 = 4$, $H_3 = 2$ and $H_4 = 1$. The CS modulus is in the conifold patch $z_C = re^{i\theta}$ and evaluations are performed to order 200 in the period series expansion Π_C . The projections on the different planes are made by fixing the values of the moduli at $r = 0.52$, $t_1 = 1.73$, $\theta = -0.496$, $t_2 = 1.295$ respectively. For this configuration, there is a dS vacuum approximately at $r = 0.63$, $t_1 = 1.55$, $\theta = -0.03$, $t_2 = 1.25$. The smallest values of ϵ in these regions are $\epsilon \sim 0.03$. A sample η eigenvalue is $\eta_{50} = -0.011$, the subindex denotes that η is computed at order 50, corresponding to the eigenvector $\eta_{min} \sim (0.67, -0.71, -0.096, -0.22)$, giving as the preferential inflationary directions along t_1 and t_2 . For the canonically normalized fields the displacements in Planck units, in the represented region, are of order $\Delta\phi_r \sim 0.124M_{Pl}$, $\Delta\phi_\theta \sim 0.58M_{Pl}$, $\Delta\phi_{t_2} \sim 0.69M_{Pl}$, $\Delta\phi_{t_1} \sim 0.65M_{Pl}$.

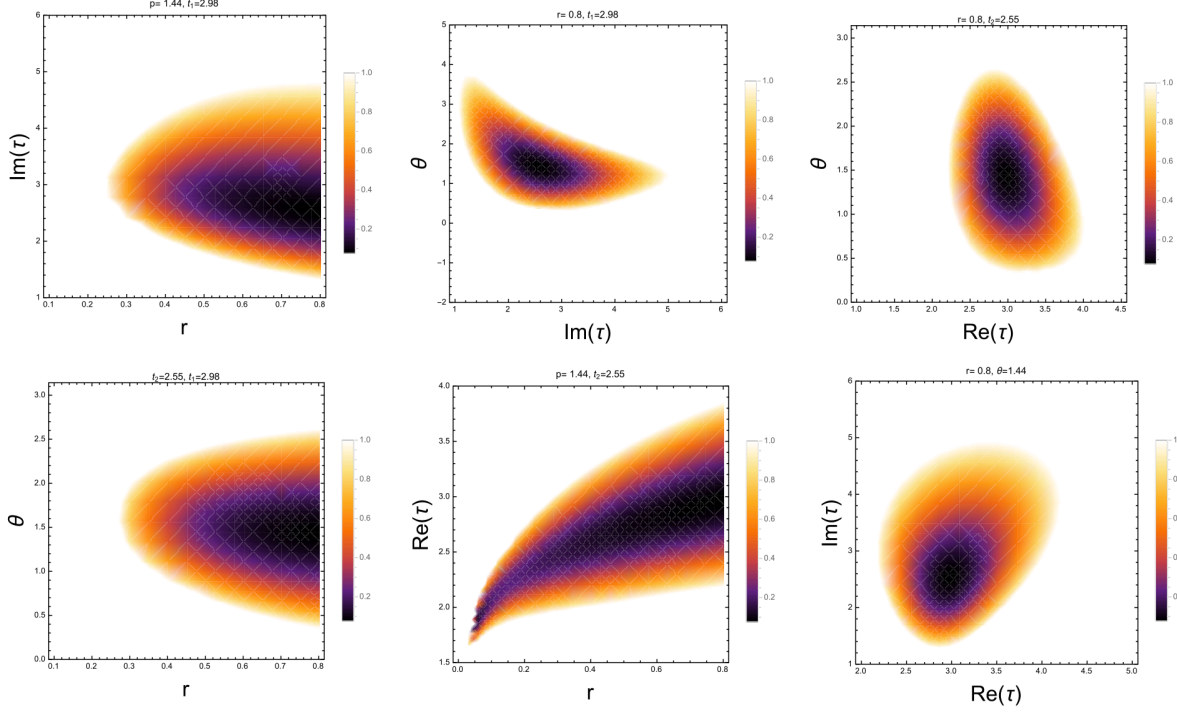


Figure 11: ϵ density plot on the six different planes for a configuration of non-zero fluxes $F_1 = 1$, $F_3 = 10$, $H_1 = 3$, $H_3 = 2$, $H_4 = 1$. The CS modulus is in the conifold patch $z_C = r e^{i\theta}$ and evaluations are performed to order 200 in the period series expansion Π_C . The planes are defined by setting two of the fields to $r_0 = 0.8$, $t_{1,0} = 2.98$, $\theta_0 = 1.44$, $t_{2,0} = 2.55$ respectively, at this point $\epsilon \sim 0.08$. For the canonically normalized fields the displacements in Planck units of the represented region are of order $\Delta\phi_r \sim 0.045 M_{Pl}$, $\Delta\phi_\theta \sim 0.065 M_{Pl}$, $\Delta\phi_{t_2} \sim 0.8 M_{Pl}$, $\Delta\phi_{t_1} \sim 0.44 M_{Pl}$. There is a minimum η eigenvalue $\eta_{100} = -0.025$ at the point $r = r_0$, $\theta = \theta_0$, $t_1 = t_{1,0}$, $t_2 = t_{2,0}$ with eigenvector $\sim (-0.98, 0.15, -0.15, 0.04)$ which signals t_1 as the dominant contribution along the inflationary direction on that point.

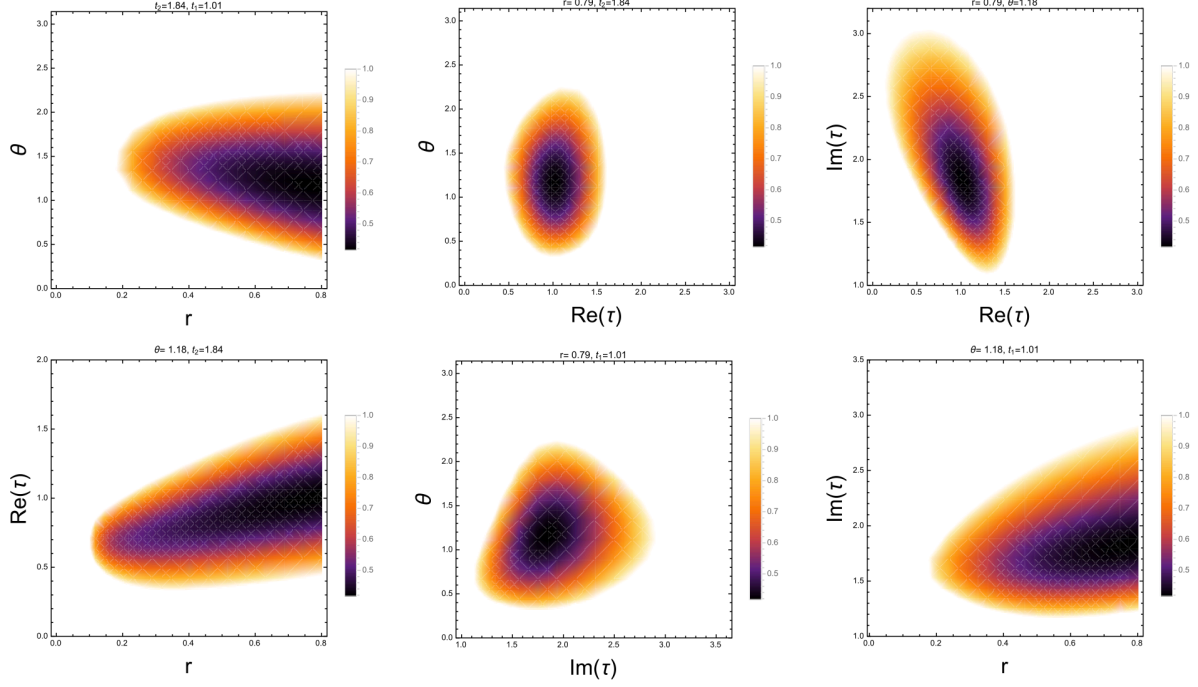


Figure 12: ϵ density plots on the six planes of two variables for a configuration of non-zero fluxes $F_1 = 2$, $F_3 = 6$, $H_1 = 4$, $H_3 = 2$, $H_4 = 2$. The CS modulus is in the conifold patch $z_C = re^{i\theta}$ and evaluations are performed to order 200 in the period series expansion Π_C . At $r = 0.79$, $t_1 = 1.01$, $\theta = 1.18$, $t_2 = 1.84$ we have $\epsilon \sim 0.417$, there are smaller values of ϵ in the orbifold convergence region. A sample η eigenvalue inside the $\epsilon < 1$ region is $\eta_{100} = -0.06$ at $r = 0.18$, $t_1 = 0.75$ and $\theta = 1.18$, $t_2 = 1.84$. The η eigenvector $-(0.8, 0.6, 0.1, 0.01)$ shows that at this point, the inflationary direction is mostly along t_1 and t_2 . For the canonically normalized fields the displacements in Planck units of the represented region are of order $\Delta\phi_r \sim 0.055M_{Pl}$, $\Delta\phi_\theta \sim 0.046M_{Pl}$, $\Delta\phi_{t_2} \sim 0.49M_{Pl}$, $\Delta\phi_{t_1} \sim 0.41M_{Pl}$.

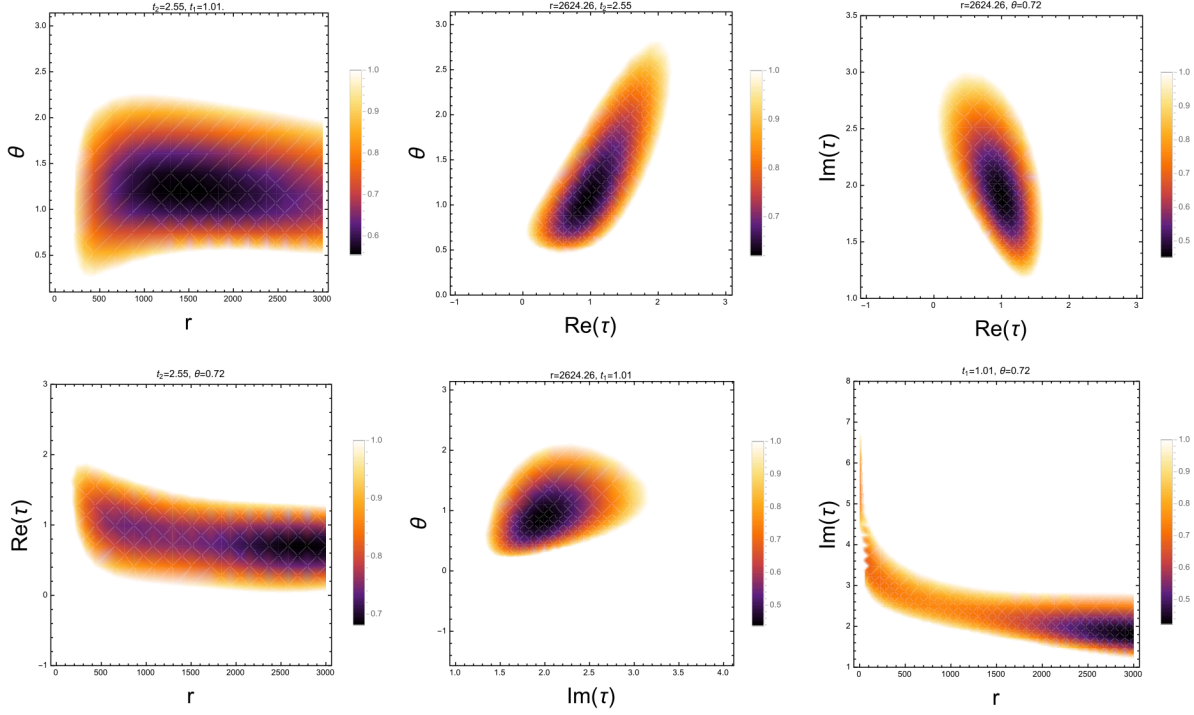


Figure 13: ϵ density plots on the six planes for the same flux configuration as in Fig. 12 in the orbifold series convergence region. The CS modulus is in the orbifold patch $z_O = r e^{i\theta}$ and evaluations are performed to order 200 in the period series expansion Π_O . A sample minimum η eigenvalue is -0.016 , for the point $t_1^0 = 1.010$, $\theta^0 = 0.7178$, $t_2^0 = 3.68$ and $r^0 = 2000$ with eigenvector $\sim (0.8, 0.6, -0.00023, 0.3)$. There is a saddle of the potential at $r = 1135.59$, $p = -1.078$, $t_1 = 0.8071$, $t_2 = 1.625$, with eigenvector $\sim (0.036, 0.0355, 0.002, -0.999)$ giving that the unstable direction is mostly θ . For the canonically normalized fields the displacements in Planck units of the represented region are $\Delta\phi_r \sim 0.037 M_{Pl}$, $\Delta\phi_\theta \sim 0.19 M_{Pl}$, $\Delta\phi_{t_2} \sim 0.49 M_{Pl}$, $\Delta\phi_{t_1} \sim 0.29 M_{Pl}$.

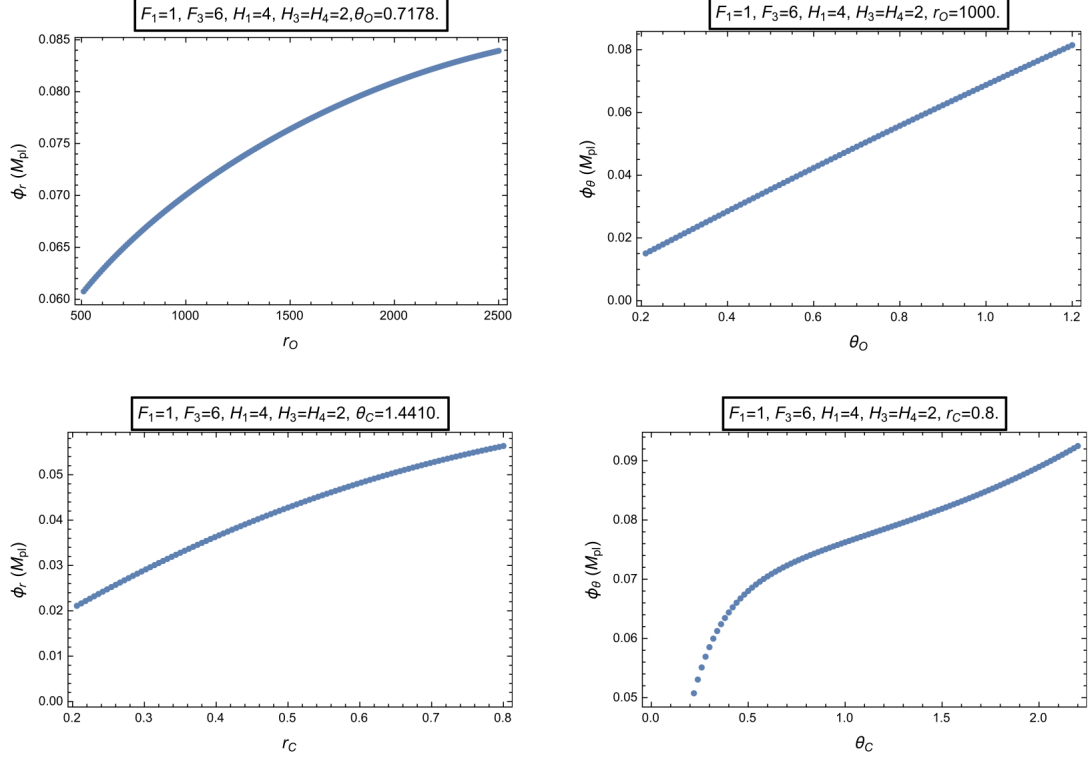


Figure 14: Trajectories of the locally normalized fields for r and θ , ϕ_r and ϕ_θ respectively, in the orbifold and conifold convergence regions. The displacement of the canonically normalized field ϕ_r is always sub-Planckian, whereas the displacement of the canonically normalized field ϕ_θ can be arbitrarily large.

We also found that for Minkowski vacua very close to the conifold point with the CS stabilised at $|z_0| \ll 1$ and with F_1, H_3, H_4 being the only non-zero fluxes, hierarchies in the physical scales exist for large values of $\frac{H_3}{H_4}$, in agreement with [1]. The vev of the axio-dilaton τ_0 is fixed for given values of F_1, H_4 while $|z_0|$ decreases according to the value for H_3 , increasing the spacetime and compactification scales' hierarchy. For these flux configurations in Section 3.1 we find an extra term in the expression for the CS value at the minimum z_0 , that changes the hierarchy by an order of magnitude. The exact vacua differ from the approximated ones, but converge to them when $\frac{H_3}{H_4}$ is increased.

In addition we studied general flux configurations, similar to those previously studied in [2] with the near conifold approximation ($z_0 \ll 1$). We review their formula for z_0 and observe that F_3 can also be tuned to achieve a small value for $|z_0|$ while keeping τ_0 constant. This provides a way of obtaining vacua with hierarchies between the 4D and 6D scales different from the ones in [1]. Again it occurs that the actual vacua differ from the vacua obtained using the near-the-conifold approximation ($z_0 \ll 1$), but in the limit of highly negative F_3 they converge to the approximated ones. In general it holds that for a generic flux configuration ensuring that $|z_0| \ll 1$ with z_0 in (3.17), the exact and approximated vacua match.

For all flux configurations with a Minkowski vacuum, we did not find slow-roll inflationary regions of the scalar potential. Numerically we observed, through multiple searches, that having both, a vacuum solution near the conifold and inflation regions, seems to be incompatible. This was done by optimising a near conifold vacuum $|z_0| < 1$ and $\epsilon < 1$ constraints varying the fluxes and the moduli. No physical solution with $g_s^{-1} = \text{Im}(\tau_0) > 1$ was found in the exploration. We further explored flux configurations with a Minkowski vacuum not necessarily closed to the conifold, but within the conifold convergence region. We looked for slow-roll regions along $\theta = \arg(z)$ taking several monodromies w.r.t. the $\theta \in [0, 2\pi)$ domain and keeping the rest of moduli fixed, but this search turned out to be unsuccessful. The modulations along θ of the scalar potential are highly affected by the power of z considered in the periods' series expansions. We also found apparent flat regions of θ , giving a small single field ϵ , but with an unstable radial direction.

We thus explored multi-field slow-roll regions, allowing all fields to evolve. The exploration was performed numerically, considering the multi-field ϵ parameter and varying all the moduli and the fluxes to optimise a minimum value of ϵ . On the phase direction, monodromies affect modulations of the potential, i.e. as θ grows the oscillations of V also increase. This implies that the only possible region with a flat potential along the CS phase lies at the bottom of the scalar potential, within the basic region of θ .

We found flux configurations with inflationary regions going from the conifold to the orbifold patch. In those regions the potential looks flat with small values of ϵ and small minimum eigenvalues of the η -parameter. In one of those cases a dS vacuum near the inflationary region was found. This is interesting as it can serve as an explicit realisation of the uplift mechanism considered in [49] once

we include stabilisation of the Kähler moduli, which could be addressed as in [35]. We computed the eigenvectors of η in the regions with slow-roll and obtained that in general, the inflationary trajectory occurs along a combination of all the moduli directions. That is, we did not find that axion monodromy inflation mostly along the phase of z , θ is realised. However, it is important to stress that we only looked for regions where the potential's slow-roll parameters (3.19) are small. It is possible that studying the more general slow-roll parameters for these type of bumpy potentials as recently considered in [48], will give rise to successful inflation. Finally, we pointed out that the ϵ values in certain patches can depend strongly on the approximation for the period series in z . Exact values of the periods are required, since one might establish false conclusions from keeping only leading terms in z .

We showed that the total displacement for the canonically normalised fields in the r ($r = r_O, r_C$ with $r_C = |z_C|$ or $r_O = |z_O|$) region (with the rest of moduli fixed) from the conifold to the orbifold is finite and smaller than a Planck unit. Thus an small excursion in Planck units of the r canonical field may include any patch of the CS moduli space. Therefore any study performed with r bounded to a single convergence critical point region is inexact for models of inflation in the CS moduli space. On the other hand, the displacement along the canonically normalised θ direction can grow unconstrained (see Figure 14).

Our results highlight the importance of considering the exact solutions for the CY periods to explore vacua and cosmological applications of the CS and dilaton moduli potential. We have found that the vacua and slow-roll conditions depend crucially on the approximation considered. It is thus important in order to study phenomenological questions to keep all necessary terms in the period expansion until convergence is achieved. Our findings indicate that one needs to consider more general slow-roll inflationary solutions where the potential can have bumpy features and give distinctive inflationary predictions as discussed recently in [48]. This can be studied at a first stage in the no-scale approximation as considered here. However a more realistic scenario will have to take into account the stabilisation of the Kähler moduli, which is a step that needs to be taken next. In addition the study of F-theory models with general axio-dilaton profile could offer new interesting possibilities. As an advantage the Kähler moduli [50] together with the CS moduli [3] can be incorporated in the effective action. CY 4-fold with more than one modulus are required, and the analysis of periods in the whole CS moduli space [34] could be useful to explore further the role of the monodromies in inflationary scenarios.

Acknowledgements

We would like to thank Alejandro Cabo Bizet, Cesar Damián, Shinji Hirano, Gabriel Lopez Cardoso, Gustavo Niz, Octavio Obregón, Fernando Quevedo and Miguel Sabido for useful discussions. We would also like to thank Shusha Parameswaran and Gianmassimo Tasinato for useful discussions and comments on the manuscript. We would like to thank specially Albrecht Klemm for many

helpful discussions, suggestions and comments on the manuscript. NC-B thanks the support of the NRF of South Africa, PROMEP and PNCB, CITMA. OL-B was partially supported by DAIP-UG project number 640/2015 and CONACYT project number 257919. The work of OL-B. and IZ was partly supported by a Royal Society Newton Mobility Grant under number NI150084. IZ thanks the Physics Department, Campus León, University of Guanajuato for hospitality during her visit.

A Transition matrices and periods on the symplectic basis

The transition matrices are computed by taking sample points lying at the intersections of the orbifold-conifold and conifold-LCS regions. We denote with S the integral symplectic basis (2.9). $M_{X,S}$ denotes the transition matrix from the coordinates X to the coordinates S . $X = C, M, O$ denotes the conifold (C), LCS (M) and orbifold (O) bases for the solutions of the PF equations, π_C (2.35), π_M (2.37), and π_O (2.36). We denote the periods expansions around the conifold, the LCS and the orbifold points in the integral symplectic basis (2.9) as Π_C , Π_M and Π_O respectively. The transition matrix from the solutions π_M to the basis (2.9) is given by

$$M_{M,S} = \begin{pmatrix} -\frac{i200}{8\pi^3}\zeta(3) & \frac{50}{24}\frac{1}{2\pi i} & 0 & \frac{1}{(2\pi i)^3} \\ \frac{50}{24} & -\frac{11}{2}\frac{1}{2\pi i} & -\frac{1}{(2\pi i)^2} & 0 \\ 1 & 0 & 0 & 0 \\ 0 & \frac{1}{2\pi i} & 0 & 0 \end{pmatrix} \quad (\text{A.1})$$

The change of basis matrix from the conifold basis π_C to the integral symplectic basis has six coefficients that can only be determined numerically, those are a, b, c, d, e and g [33]. In our calculations we have determined the elements of the matrix with 40 digits of precision to be ¹⁵

$$M_{C,S} = \begin{pmatrix} 0 & -\frac{\sqrt{5}}{2\pi}i & 0 & 0 \\ a - \frac{11}{2}ig & b - \frac{11}{2}ih & c - \frac{11}{2}ir & 0 \\ d & e & f & -\frac{\sqrt{5}}{(2\pi i)^2} \\ ig & ih & ir & 0 \end{pmatrix} \quad (\text{A.2})$$

The transition matrix $M_{O,S}$ between the orbifold basis and the integral symplectic basis Π_O (2.9)

¹⁵The elements of $M_{C,S}$ given till order 20 are: $a = 6.1950162771495748881$, $b = 1.01660471670258207478$, $c = -0.14088997944883090936$, $d = 1.0707258684301558006$, $e = -0.024707613804484718111$, $f = 0.0057845115995744470969$, $g = 1.2935739845041086377$, $h = 0.15076669512354730097$, $r = -0.027792180016865244887$.

satisfying $\Pi_O = M_{O,S}\pi_O$ has an inverse

$$M_{O,S}^{-1} = \begin{pmatrix} -\frac{16e^{\frac{2\pi i}{5}}\pi^4}{(e^{\frac{2\pi i}{5}}-1)\Gamma[\frac{1}{5}]^5} & -\frac{16e^{\frac{2\pi i}{5}}\pi^4}{(e^{\frac{2\pi i}{5}}-1)^2\Gamma[\frac{1}{5}]^5} & \frac{80e^{\frac{2\pi i}{5}}(1-e^{\frac{2\pi i}{5}}+e^{\frac{4\pi i}{5}})\pi^4}{(e^{\frac{2\pi i}{5}}-1)^4\Gamma[\frac{1}{5}]^5} & -\frac{16e^{\frac{2\pi i}{5}}(-3+8e^{\frac{2\pi i}{5}})\pi^4}{(e^{\frac{2\pi i}{5}}-1)^3\Gamma[\frac{1}{5}]^5} \\ -\frac{16e^{\frac{4\pi i}{5}}\pi^4}{(e^{\frac{4\pi i}{5}}-1)\Gamma[\frac{2}{5}]^5} & -\frac{16e^{\frac{4\pi i}{5}}\pi^4}{(e^{\frac{4\pi i}{5}}-1)^2\Gamma[\frac{2}{5}]^5} & \frac{80e^{\frac{4\pi i}{5}}(1+e^{-\frac{2\pi i}{5}}-e^{\frac{4\pi i}{5}})\pi^4}{(e^{\frac{4\pi i}{5}}-1)^4\Gamma[\frac{2}{5}]^5} & -\frac{16e^{\frac{4\pi i}{5}}(-3+8e^{\frac{4\pi i}{5}})\pi^4}{(e^{\frac{4\pi i}{5}}-1)^3\Gamma[\frac{2}{5}]^5} \\ -\frac{32e^{-\frac{4\pi i}{5}}\pi^4}{(e^{-\frac{4\pi i}{5}}-1)\Gamma[\frac{3}{5}]^5} & -\frac{32e^{-\frac{4\pi i}{5}}\pi^4}{(e^{-\frac{4\pi i}{5}}-1)^2\Gamma[\frac{3}{5}]^5} & \frac{160e^{-\frac{4\pi i}{5}}(1+e^{\frac{2\pi i}{5}}-e^{-\frac{4\pi i}{5}})\pi^4}{(e^{-\frac{4\pi i}{5}}-1)^4\Gamma[\frac{3}{5}]^5} & -\frac{32e^{-\frac{4\pi i}{5}}(-3+8e^{-\frac{4\pi i}{5}})\pi^4}{(e^{-\frac{4\pi i}{5}}-1)^3\Gamma[\frac{3}{5}]^5} \\ -\frac{96e^{-\frac{2\pi i}{5}}\pi^4}{(e^{-\frac{2\pi i}{5}}-1)\Gamma[\frac{4}{5}]^5} & -\frac{96e^{-\frac{2\pi i}{5}}\pi^4}{(e^{-\frac{2\pi i}{5}}-1)^2\Gamma[\frac{4}{5}]^5} & \frac{480e^{-\frac{2\pi i}{5}}(1-e^{-\frac{2\pi i}{5}}+e^{-\frac{4\pi i}{5}})\pi^4}{(e^{-\frac{2\pi i}{5}}-1)^4\Gamma[\frac{4}{5}]^5} & -\frac{96e^{-\frac{2\pi i}{5}}(-3+8e^{-\frac{2\pi i}{5}})\pi^4}{(e^{-\frac{2\pi i}{5}}-1)^3\Gamma[\frac{4}{5}]^5} \end{pmatrix} \quad (\text{A.3})$$

The transition matrix given numerically reads

$$M_{O,S} = \begin{pmatrix} 0.587512i & -0.171576i & 0.011701i & -0.000103i \\ 1.462844 - 2.338201i & -0.038521 + 0.260823114i & -0.002627 - 0.017787i & 0.000256 + 0.000409i \\ 0.404320 - 0.293756i & -0.027874 + 0.085788i & -0.001901 - 0.005850i & 0.000071 + 0.000051i \\ 0.425127i & -0.047422i & 0.003234i & -0.000074i \end{pmatrix} \quad (\text{A.4})$$

We give the first three order of the periods vs. z_C on the integral symplectic basis. This expression is obtained by acting with $M_{C,S}$ on π_C in (2.35). The period vector $\Pi_C = (\Pi_{C,1}, \Pi_{C,2}, \Pi_{C,3}, \Pi_{C,4})$ has components

$$\begin{aligned} \Pi_{C,1} &= -0.355881iz - 0.249117iz^2 - 0.194548iz^3 + O(z^4), \\ \Pi_{C,2} &= 6.19502 - 7.11466i + (1.0166 - 0.829217i)z + (0.570733 - 0.427595i)z^2 \\ &\quad + (0.401804 - 0.287548i)z^3 + O(z^4), \\ \Pi_{C,3} &= 1.07073 + \alpha z - 0.011511z^2 - 0.006565z^3 \\ &\quad - \frac{\ln z}{2\pi i}(-2\pi i\beta z - 0.249117iz^2 - 0.194548iz^3) + O(z^4), \\ \Pi_{C,4} &= 1.29357i + 0.150767iz + 0.0777445iz^2 + 0.0522815iz^3 + O(z^4). \end{aligned} \quad (\text{A.5})$$

Let us define here the coefficients as $\alpha = -0.024708$ and $\beta = 0.056640$, these are employed in Section 3.1. Observe that the monodromy is explicit because $\Pi_C^3 = -\Pi_C^1 \ln z / (2\pi i) + Q(z)$. The periods vs. z_O on the integral symplectic basis are obtained by $\Pi_O = M_{O,S}\pi_O$ in (2.36). The period vector $\Pi_O = (\Pi_{O,1}, \Pi_{O,2}, \Pi_{O,3}, \Pi_{O,4})$ has components

$$\begin{aligned} \Pi_{O,1} &= 0.587512iz^{1/5} - 0.171576iz^{2/5} + 0.0117008iz^{3/5} + O(z^{4/5}), \\ \Pi_{O,2} &= (1.46284 - 2.3382i)z^{1/5} - (0.0385212 - 0.260823i)z^{2/5} \\ &\quad - (0.002627 + 0.0177871i)z^{3/5} + O(z^{4/5}), \\ \Pi_{O,3} &= (0.40432 - 0.293756i)z^{1/5} - (0.0278742 - 0.0857879i)z^{2/5} \\ &\quad - (0.00190091 + 0.00585041i)z^{3/5} + O(z^{4/5}), \\ \Pi_{O,4} &= 0.425127iz^{1/5} - 0.0474224iz^{2/5} + 0.00323402iz^{3/5} + O(z^{4/5}). \end{aligned} \quad (\text{A.6})$$

The periods vs. z_M on the integral symplectic basis are obtained by acting with $M_{M,S}$ on π_M in (2.37). To obtain $\Pi_M = (\Pi_{M,1}, \Pi_{M,2}, \Pi_{M,3}, \Pi_{M,4})$ with

$$\begin{aligned}
\Pi_{M,1} &= -\frac{25i\zeta(3)}{\pi^3} + \left(-\frac{2875i}{4\pi^3} - \frac{9625i}{2\pi} - \frac{3000i\zeta(3)}{\pi^3}\right)z + \left(-\frac{16491875i}{32\pi^3} - \frac{6751875i}{8\pi} - \frac{2835000i\zeta(3)}{\pi^3}\right)z^2 \\
&+ \ln z \left(-\frac{25}{24\pi}i + \left(\frac{2875}{8\pi^3} - \frac{125}{\pi}\right)iz + \left(\frac{21040875}{32\pi^3} - \frac{118125}{\pi}\right)iz^2\right) \\
&+ \frac{5i}{16\pi^3} \ln z^2 (770z + 810225z^2) + \frac{i}{48\pi^3} \ln z^3 (1 + 5!z + \frac{10!}{2^5}z^2) + O(z^3), \\
\Pi_{M,2} &= \frac{25}{12} + \left(250 + \frac{2875}{4\pi^2} + \frac{4235i}{2\pi}\right)z + \left(236250 + \frac{21040875}{16\pi^2} + \frac{8912475i}{4\pi}\right)z^2, \\
&+ \ln z \left(\frac{11i}{4\pi} + z\left(\frac{1925}{2\pi^2} + \frac{330i}{\pi}\right) + z^2\left(\frac{4051125}{4\pi^2} + \frac{311850i}{\pi}\right)\right) + \\
&+ \frac{5}{8\pi^2} \ln z^2 \left(1 + 5!z + \frac{10!}{2^5}z^2\right) + O(z^3), \\
\Pi_{M,3} &= 1 + 5!z + \frac{10!}{2^5}z^2 + O(z^3), \\
\Pi_{M,4} &= \frac{1}{2\pi i} (770z + 810225z^2)z + \frac{\ln z}{2\pi i} (1 + 5!z + \frac{10!}{2^5}z^2) + O(z^3).
\end{aligned} \tag{A.7}$$

B Hierarchies

Let us summarise the correction to the hierarchy formula of [1] using the notation of that paper. The non-zero fluxes in their notation are M, K, K' which we denote as F_1, H_3, H_4 . The four components of the periods are described on those coordinates as

$$\Pi(z) = (z, z'(z), \mathcal{G}(z), \mathcal{G}'(z)), \tag{B.1}$$

while we note them as Π_i . The third component of the period vector has in general the properties [1]

$$\mathcal{G}(z) = \frac{z \ln z}{2\pi i} + \text{hol.}, \quad \mathcal{G}(0) \neq 0, \quad \partial_z \mathcal{G}(z) = \frac{\ln z}{2\pi i} + \delta_1(z). \tag{B.2}$$

Closed to the conifold when $z \rightarrow 0$ we evaluate the following quantities

$$\begin{aligned}
\bar{\Pi}_0 \Sigma \Pi_0 &= \bar{z}'(0) \mathcal{G}'(0) - \bar{\mathcal{G}}'(0) z'(0), \\
\bar{\Pi}_0 \Sigma \partial_z \Pi_0 &= \bar{\mathcal{G}}(0) - \bar{z}'(0) \partial_z \mathcal{G}'(0) - \bar{\mathcal{G}}'(0) \partial_z z'(0), \\
\tau_0 &= \frac{M \bar{\mathcal{G}}(0)}{K' \bar{z}'(0)}, \\
\partial_z K_0 &= \frac{\bar{\Pi}_0 \Sigma \partial_z \Pi_0}{\bar{\Pi}_0 \Sigma \Pi_0}, \\
W_0 &= M \mathcal{G}(0) - \tau_0 K' z'(0).
\end{aligned}$$

This will give a covariant derivate of W

$$\begin{aligned}
D_z W &= M \left(\frac{\ln z}{2\pi i} + \delta_1(0) \right) - \tau_0(K + K' \dot{z}'(0)) + \partial_z K_0 W_0 + O(z), \\
&= M \frac{\ln z}{2\pi i} - \tau_0 K + b_0 + O(z), \\
b_0 &= M \delta_1(0) - \tau_0 K' \dot{z}'(0) + \partial_z K_0 W_0, \\
\Delta_0 &= b_0/M = \delta_1(0) - \frac{\bar{\mathcal{G}}(0)}{\bar{z}'(0)} \partial_z z'(0) + \partial_z K_0 \left(\mathcal{G}(0) - \frac{\bar{\mathcal{G}}(0)}{\bar{z}'(0)} z'(0) \right).
\end{aligned} \tag{B.3}$$

This translates in that there is a hierarchy given by

$$\begin{aligned}
z_0 &\sim \exp 2\pi i \left(\frac{\tau_0 K}{M} - \Delta_0 \right), \\
&\sim \exp 2\pi i \left(\frac{K \bar{\mathcal{G}}(0)}{K' \bar{z}'(0)} - \Delta_0 \right).
\end{aligned} \tag{B.4}$$

The previous formula adds a factor $\exp(-2\pi i \Delta_0)$ w.r.t. to (3.18) in [1] this constitutes a correction to the hierarchy between the 4D and 6D scales, which is independent of the fluxes.

C Effect of monodromies on the scalar potential

The existence of inflationary regions due to monodromies has been widely explored in the last years. A logical strategy is to look for Minkowski vacua (especially in no-scale models as in the present case) and move around the moduli vevs in order to find flat regions in the potential. In Section 3.3 we looked at the profile of the scalar potential in the complex structure phase direction θ , while keeping all other moduli frozen at their vevs. We found that the amplitude of oscillations in the scalar potential along θ increased as we encircled the conifold. Here we present an alternative way of moving away from the Minkowski minimum in z along the direction determined by $D_\tau W = 0$, implying a transformation of the axio-dilaton in the trajectory.

In the examples studied and presented in Section 3.3, we saw that moving away from the vacuum in the θ -direction, the scalar potential starts oscillating and the amplitude of the oscillations are not constant as would be expected from an effective potential of the form

$$V \sim \Lambda \sin \left(\frac{\theta}{f} \right). \tag{C.1}$$

Here we present an analytical description of this feature. For this we study a displacement in the direction defined by $D_\tau W = 0$ while performing monodromies $z \rightarrow e^{2\pi i n} z, n \in \mathbb{Z}$ around the conifold. This is a good approximation for small values of g_s and τ fixed at its value at the Minkowski minimum. However we'll see that far from the vacuum, g_s starts growing leading the potential to an unphysical region. Under n -monodromies the superpotential W transforms as

$$W \rightarrow W - n G_1 \Pi_1 \equiv W - n g, \tag{C.2}$$

and by keeping $D_\tau W = 0$ after monodromies, the dilaton transforms as

$$\tau_0 \rightarrow \tau' = \frac{\tau_0 \bar{\mathcal{H}} - n \bar{f}}{\bar{\mathcal{H}} - n \bar{h}}, \quad (\text{C.3})$$

where $\mathcal{H} = H^\dagger \Sigma \bar{\Pi}$, $f = F_1 \Pi_1$ and $h = H_1 \Pi_1$. Observe that it is not possible to perform a $SL(2, \mathbb{Z})$ transformation of τ while keeping $D_\tau W = 0$. i.e. the τ -transformation given by (C.3) is not an $SL(2, \mathbb{Z})$ -transformation.

The transformed superpotential, over a region on which $D_\tau W = 0$, is given by

$$\begin{aligned} W &\rightarrow W(\tau') - ng(\tau') \\ &= \omega(n, \bar{z}_0) \left[W(\tau_0, z_0) - \frac{n}{\bar{\mathcal{H}}} (\bar{h} \mathcal{F} - \bar{f} \mathcal{H} + \bar{\mathcal{H}} g(\tau_0)) \right] \\ &\equiv \omega(W_0 + \delta W) \end{aligned} \quad (\text{C.4})$$

where

$$\omega(n, \bar{z}_0) = \frac{\bar{\mathcal{H}}}{\bar{\mathcal{H}} - n \bar{h}}, \quad (\text{C.5})$$

and $\mathcal{F} = F^\dagger \Sigma \Pi$. For each value of n , the values of W and the rest of terms $(\mathcal{H}, \mathcal{F}, h, f)$ are fixed at the minimum point z_0 and τ_0 . Now, notice that since $D_z W_0 = 0$ and $D_\tau W = 0$ in $\tau = \tau'$ we have that

$$V = e^{\mathcal{K}(z_0, \tau'(n))} |D_z(\omega \delta W)|_{z_0}^2 K^{z\bar{z}}(z_0, \bar{z}_0), \quad (\text{C.6})$$

from which we can read that the only contribution to the scalar potential comes from the complex structure's Kähler derivative. The final expression for V is

$$V = \frac{ig_s(n)}{2} \frac{1}{\Pi^\dagger \Sigma \bar{\Pi}(z_0)} |D_z \xi|_{z_0}^2 K_0^{z\bar{z}} \left| \frac{n}{\bar{\mathcal{H}}_0 - n \bar{h}_0} \right|^2, \quad (\text{C.7})$$

where

$$\xi = 2i \text{Im}(f \bar{\mathcal{H}} - h \bar{\mathcal{F}}), \quad (\text{C.8})$$

and

$$\frac{1}{g_s(n)} = \text{Im} \frac{|\mathcal{H}|^2 \bar{\mathcal{F}} \mathcal{H} + n (\bar{\mathcal{H}}^2 \mathcal{F} h - \bar{f} \mathcal{H} |\mathcal{H}|^2)}{|\mathcal{H}|^2 |\bar{\mathcal{H}} - n \bar{h}|^2}. \quad (\text{C.9})$$

Notice the following:

1. For large n , g_s tends to infinite (see also (C.3)), implying that our perturbative analysis is only valid from $n = 0$ to some finite n . Actually for n satisfying

$$|\mathcal{H}|^4 n^2 + [-2|\mathcal{H}|^2 \text{Re}(\mathcal{H} \bar{h}) + \text{Im}(\bar{\mathcal{H}}^2 \mathcal{F} h - \mathcal{H}^2 \bar{\mathcal{H}} f)] n + |\mathcal{H}|^2 [|h|^2 - \text{Im}(\bar{\mathcal{F}} \mathcal{H})] < 0, \quad (\text{C.10})$$

at $z = z_0$, for which $g_s < 1$.

2. From relation (C.3), it is straightforward to see that positive monodromies will lead to a string coupling with the opposite sign with respect to that at the minimum. Hence, if we start in a perturbative regime, for some positive n , we shall leave the physical region. This however does not happen for negative monodromies.

By substituting the value of $g_s(n)$ in V , we get

$$V = \frac{n^2 C}{A + Bn}(z_0) \quad (\text{C.11})$$

with n negative and A , B and C functions valued at z_0 given by

$$\begin{aligned} C(z_0) &= \frac{i|\mathcal{H}|^2}{\Pi^\dagger \Sigma \Pi} |D_z \xi|_{z_0}^2 K_0^{z\bar{z}}, \\ B(z_0) &= \mathcal{H}^2 \mathcal{F} h - \bar{f} \mathcal{H} |\mathcal{H}|^2, \\ A(z_0) &= 2 \operatorname{Im}(|\mathcal{H}|^2 \bar{\mathcal{F}} \mathcal{H}). \end{aligned} \quad (\text{C.12})$$

These values of the scalar potential at entire displacements of θ , show that for each shift on the phase $\theta \rightarrow \theta + 2\pi$, the scalar potential increases its value. The analysis breaks down as g_s becomes larger than unity or the scalar potential becomes negative, showing that our assumption on $D_\tau W = 0$ cannot be kept on the whole physical moduli space. Between each consecutive value of n the scalar potential oscillates with a minimum for some value of θ in the interval $[\theta + 2\pi n, \theta + 2\pi(n+1))$. This shows that for the given trajectory in the moduli space, one expects an increase in the oscillations' amplitude of the scalar potential.

References

- [1] S. B. Giddings, S. Kachru, and J. Polchinski, “Hierarchies from fluxes in string compactifications,” *Phys.Rev.* **D66** (2002) 106006, [hep-th/0105097](#).
- [2] P. Ahlqvist, B. R. Greene, D. Kagan, E. A. Lim, S. Sarangi, *et. al.*, “Conifolds and Tunneling in the String Landscape,” *JHEP* **1103** (2011) 119, [1011.6588](#).
- [3] S. Gukov, C. Vafa, and E. Witten, “CFT’s from Calabi-Yau four folds,” *Nucl. Phys.* **B584** (2000) 69–108, [hep-th/9906070](#). [Erratum: *Nucl. Phys.* **B608**, 477(2001)].
- [4] G. Curio, A. Klemm, D. Lust, and S. Theisen, “On the vacuum structure of type II string compactifications on Calabi-Yau spaces with H fluxes,” *Nucl. Phys.* **B609** (2001) 3–45, [hep-th/0012213](#).
- [5] I. R. Klebanov and M. J. Strassler, “Supergravity and a confining gauge theory: Duality cascades and chi SB resolution of naked singularities,” *JHEP* **08** (2000) 052, [hep-th/0007191](#).

- [6] S. Kachru, R. Kallosh, A. D. Linde, and S. P. Trivedi, “De Sitter vacua in string theory,” *Phys. Rev.* **D68** (2003) 046005, [hep-th/0301240](#).
- [7] K. Kooner, S. Parameswaran, and I. Zavala, “Warping the Weak Gravity Conjecture,” [1509.07049](#).
- [8] E. Silverstein and A. Westphal, “Monodromy in the CMB: Gravity Waves and String Inflation,” *Phys. Rev.* **D78** (2008) 106003, [0803.3085](#).
- [9] L. McAllister, E. Silverstein, and A. Westphal, “Gravity Waves and Linear Inflation from Axion Monodromy,” *Phys. Rev.* **D82** (2010) 046003, [0808.0706](#).
- [10] M. Cicoli, C. P. Burgess, and F. Quevedo, “Fibre Inflation: Observable Gravity Waves from IIB String Compactifications,” *JCAP* **0903** (2009) 013, [0808.0691](#).
- [11] A. Avgoustidis and I. Zavala, “Warped Wilson Line DBI Inflation,” *JCAP* **0901** (2009) 045, [0810.5001](#).
- [12] D. H. Lyth, “What would we learn by detecting a gravitational wave signal in the cosmic microwave background anisotropy?,” *Phys.Rev.Lett.* **78** (1997) 1861–1863, [hep-ph/9606387](#).
- [13] K. Freese, J. A. Frieman, and A. V. Olinto, “Natural inflation with pseudo - Nambu-Goldstone bosons,” *Phys. Rev. Lett.* **65** (1990) 3233–3236.
- [14] A. Linde, “Chaotic inflation,” *Physics Letters B* **129** (1983), no. 3 177 – 181.
- [15] N. Kaloper and L. Sorbo, “A Natural Framework for Chaotic Inflation,” *Phys. Rev. Lett.* **102** (2009) 121301, [0811.1989](#).
- [16] F. Marchesano, G. Shiu, and A. M. Uranga, “F-term Axion Monodromy Inflation,” *JHEP* **09** (2014) 184, [1404.3040](#).
- [17] R. Blumenhagen and E. Plauschinn, “Towards Universal Axion Inflation and Reheating in String Theory,” *Phys. Lett.* **B736** (2014) 482–487, [1404.3542](#).
- [18] R. Blumenhagen, D. Herschmann, and E. Plauschinn, “The Challenge of Realizing F-term Axion Monodromy Inflation in String Theory,” *JHEP* **01** (2015) 007, [1409.7075](#).
- [19] A. Hebecker, P. Mangat, F. Rompineve, and L. T. Witkowski, “Tuning and Backreaction in F-term Axion Monodromy Inflation,” *Nucl.Phys.* **B894** (2015) 456–495, [1411.2032](#).
- [20] D. Escobar, A. Landete, F. Marchesano, and D. Regalado, “Large field inflation from D-branes,” [1505.07871](#).
- [21] D. Andriot, “A no-go theorem for monodromy inflation,” [1510.02005](#).

- [22] D. Escobar, A. Landete, F. Marchesano, and D. Regalado, “D6-branes and axion monodromy inflation,” 1511.08820.
- [23] A. Hebecker, J. Moritz, A. Westphal, and L. T. Witkowski, “Axion Monodromy Inflation with Warped KK-Modes,” 1512.04463.
- [24] R. Blumenhagen, A. Font, M. Fuchs, D. Herschmann, E. Plauschinn, Y. Sekiguchi, and F. Wolf, “A Flux-Scaling Scenario for High-Scale Moduli Stabilization in String Theory,” *Nucl. Phys.* **B897** (2015) 500–554, 1503.07634.
- [25] R. Blumenhagen, A. Font, M. Fuchs, D. Herschmann, and E. Plauschinn, “Large field inflation and string moduli stabilization,” in *18th International Conference From the Planck Scale to the Electroweak Scale (Planck 2015) Ioannina, Greece, May 25-29, 2015*, 2015. 1510.04059.
- [26] R. Blumenhagen, C. Damian, A. Font, D. Herschmann, and R. Sun, “The Flux-Scaling Scenario: De Sitter Uplift and Axion Inflation,” 1510.01522.
- [27] A. Hebecker, P. Mangat, F. Rompineve, and L. T. Witkowski, “Winding out of the Swamp: Evading the Weak Gravity Conjecture with F-term Winding Inflation?,” 1503.07912.
- [28] T. Kobayashi, A. Oikawa, and H. Otsuka, “New potentials for string axion inflation,” 1510.08768.
- [29] A. Landman, “On the Picard-Lefschetz transformation for algebraic manifolds acquiring general singularities,” *Trans. Amer. Math. Soc.* **B609** (1973) 89126.
- [30] A. Hebecker, F. Rompineve, and A. Westphal, “Axion Monodromy and the Weak Gravity Conjecture,” 1512.03768.
- [31] I. Garcia-Etxebarria, T. W. Grimm, and I. Valenzuela, “Special Points of Inflation in Flux Compactifications,” *Nucl. Phys.* **B899** (2015) 414–443, 1412.5537.
- [32] P. Candelas, X. C. De La Ossa, P. S. Green, and L. Parkes, “A Pair of Calabi-Yau manifolds as an exactly soluble superconformal theory,” *Nucl.Phys.* **B359** (1991) 21–74.
- [33] M.-x. Huang, A. Klemm, and S. Quackenbush, “Topological string theory on compact Calabi-Yau: Modularity and boundary conditions,” *Lect. Notes Phys.* **757** (2009) 45–102, hep-th/0612125.
- [34] N. C. Bizet, A. Klemm, and D. V. Lopes, “Landscaping with fluxes and the E8 Yukawa Point in F-theory,” 1404.7645.
- [35] F. Denef, M. R. Douglas, B. Florea, A. Grassi, and S. Kachru, “Fixing all moduli in a simple f-theory compactification,” *Adv. Theor. Math. Phys.* **9** (2005), no. 6 861–929, hep-th/0503124.

- [36] T. C. Bachlechner, C. Long, and L. McAllister, “Planckian Axions in String Theory,” *JHEP* **12** (2015) 042, 1412.1093.
- [37] C. Long, L. McAllister, and J. Stout, “Systematics of Axion Inflation in Calabi-Yau Hypersurfaces,” 1603.01259.
- [38] P. Candelas, X. C. De la Ossa, P. S. Green, and L. Parkes, “An Exactly soluble superconformal theory from a mirror pair of Calabi-Yau manifolds,” *Phys.Lett.* **B258** (1991) 118–126.
- [39] P. Candelas and X. de la Ossa, “Moduli Space of Calabi-Yau Manifolds,” *Nucl. Phys.* **B355** (1991) 455–481.
- [40] S. Hosono, A. Klemm, S. Theisen, and S.-T. Yau, “Mirror symmetry, mirror map and applications to complete intersection Calabi-Yau spaces,” *Nucl. Phys.* **B433** (1995) 501–554, hep-th/9406055.
- [41] I. Brunner and K. Hori, “Orientifolds and mirror symmetry,” *JHEP* **0411** (2004) 005, hep-th/0303135.
- [42] R. Blumenhagen, V. Braun, T. W. Grimm, and T. Weigand, “GUTs in Type IIB Orientifold Compactifications,” *Nucl.Phys.* **B815** (2009) 1–94, 0811.2936.
- [43] F. Denef, “Les Houches Lectures on Constructing String Vacua,” 0803.1194.
- [44] B. R. Greene and M. R. Plesser, “(2,2) AND (2,0) SUPERCONFORMAL ORBIFOLDS,” .
- [45] J. Polchinski, *String Theory: Volumes 1&2*. Cambridge Monographs on Mathematical Physics. Cambridge University Press, 1998.
- [46] P. Candelas and X. C. de la Ossa, “Comments on Conifolds,” *Nucl. Phys.* **B342** (1990) 246–268.
- [47] L. Covi, M. Gomez-Reino, C. Gross, J. Louis, G. A. Palma, and C. A. Scrucca, “Constraints on modular inflation in supergravity and string theory,” *JHEP* **08** (2008) 055, 0805.3290.
- [48] S. Parameswaran, G. Tasinato, and I. Zavala, “Subleading Effects and the Field Range in Axion Inflation,” 1602.02812.
- [49] A. Saltman and E. Silverstein, “The Scaling of the no scale potential and de Sitter model building,” *JHEP* **11** (2004) 066, hep-th/0402135.
- [50] E. Witten, “Nonperturbative superpotentials in string theory,” *Nucl. Phys.* **B474** (1996) 343–360, hep-th/9604030.